STRUCTURE AND ENVIRONMENT

Contents

structure

environment

STRUCTURE AND ENVIRONMENT

archtitecture, construction, environmental engineering, energy

"Structure and Environment" is the technical journal with the wide spectrum such as architecture, civil engineering, environmental engineering and energy. It is understood in the wide sense as the process of construction, starting from conceiving the project, initial stage of project preparation (architecture, surveying, geology, physics of structures, construction, utilities), carrying it out in the field (civil engineering, technologies in construction and utilities, construction materials, automation and control process), use (environmental engineering, macro-and microclimate, healthy and intelligent building, clean environment, energetics) up to final stage of closing the cycle (recycling, waste treatment engineering, renewable energy sources, balanced development). Although the spectrum of these themes is so wide, its aim is one: construction of the beautiful shape, which is functional, user friendly, safe, stable, healthy, environment friendly, assureing balanced development. Although the title and design of this journal implies division into two parts: structure and environment, it actually pertains one goal: proper and approved by the society shape of the structure in the environment and the environment within the structure.

The range of journal's contributors with such a wide thematic spectrum is very wide: scientists, researchers, Ph. D. - candidates, students, producers, project engineers, project managers, participants of developments projects, users, patent participants, who are applying and exploring the possibility of new, often modern or innovative solutions. Therefore, the main task for which the SaE journal was created is to become the link between the innovative thoughts, research and development, use and the healthy impact on creativity. It is up to us, if we will take this challenge and actively participate in fulfilling its objectives. I invite you cordially to do so.

„Struktura i Środowisko" jest czasopismem technicznym o szerokim zakresie tematycznym, obejmującym architekturę, budownictwo, inżynierię środowiska, energetykę. To zagadnienia szeroko pojętego budownictwa od przygotowania projektu (architektura, geodezja, geologia, fizyka budowli, konstrukcje, instalacje), poprzez realizację (budownictwo, technologie budowlane i instalacyjne, materiały budowlane, automatyka i sterowanie), eksploatację (inżynieria środowiska, makro- i mikroklimat, zdrowy i inteligentny budynek, czyste środowisko, oszczędność energii, energetyka) do zamknięcia cyklu (recykling, inżynieria unieszkodliwiania odpadów, odnawialne źródła energii, zrównoważony rozwój). Mimo takiego szerokiego podejścia tematycznego, wszystko wiąże jeden cel: budowla — o pięknej bryle, funkcjonalna, przyjazna, bezpieczna, trwała, zdrowa, nie degradująca środowiska, zapewniająca zrównoważony rozwój. Mimo, że tytuł i układ czasopisma sugerują podział na dwa zagadnienia: strukturę i środowisko, w istocie dotyczy jednej idei — właściwego i akceptowalnego przez społeczeństwo kształtowania struktury w środowisku i środowiska w strukturze.

Forum czasopisma o takim zakresie tematycznym jest bardzo szerokie; naukowcy, badacze, doktoranci, studenci, producenci, inżynierowie, projektanci i wykonawcy, uczestnicy projektów rozwojowych, patentujący, wdrażający i eksploatujący nowe, często innowacyjne, rozwiązania. Dlatego głównym celem, dla którego „SaE" zostało stworzone jest spełnienie roli komunikatora myśli twórczej, doświadczeń badawczych, efektów praktycznych i zwrotnego oddziaływania na twórczość. Nam pozostaje tylko decyzja czy włączyć się w realizację tego celu — do czego serdecznie namawiam.

Jerzy Zb. Piotrowski

GRZEGORZ STELMASZCZYK
PRZEMYSŁAW ŚWIERCZ

Kielce University of Technology,
Al. Tysiąclecia Państwa Polskiego 7,
25-314 Kielce, Poland,
e-mail: zmsgs@tu.kielce.pl

EVALUATION OF CALCAREOUS AGGREGATE USABILITY FOR FROST RESISTANCE CONCRETES

A b s t r a c t

The durability of concrete structures exposed to water and frost action depends, among others, on physical properties of coarse aggregate, primarily on its porosity, dimensions, shapes and pores continuity.
The paper presents the results of investigations into the diversified physical properties of the rock and calcareous aggregate from the same deposit with respect to their durability under cyclic freezing and thawing conditions.

Keywords: concrete frost resistance, calcareous aggregate

1. Introduction

The freeze/thaw resistance of the concrete is decisive for the durability of structures of this material exposed to water, frost action, and often also deicing salts. Deterioration of concrete structures under winter conditions is related to the microstructure of hardened concrete. Obtaining frost resistance structure of the cement paste by means of its aeration and also proper quantitative and qualitative selection of components causes hardly any problems in practice. On the other hand, the choice of appropriate coarse aggregate, which constitutes approx. 50% of the total concrete volume, often presents serious difficulties and may result in many unpredictable defects that are revealed in the operation of such structure [1], [2].

Physical properties, in particular porosity, absorbability or size and geometrical arrangement of pores are decisive as regards aggregate usability for frost resistance concretes. For practical purposes, the stability of those parameters in different aggregate batches is also important. It is often difficult to satisfy the above-mentioned condition for mines quarrying stratified deposits of different origin and various physical properties. That refers particularly to calcareous rocks.

The paper presents results of investigations into physical features of calcareous aggregate from a deposit of diversified properties with respect to aggregate usability for frost resistance concretes. Aggregate and rock material samples used in investigations were taken from one of limestone deposits, in operation for a few dozen years, in the Swietokrzyski Region.

2. Range and methods of investigations

The range of investigations covered the assessment of changeability of physical properties of calcareous aggregate from the same deposit as regards its usability for concretes exposed to the action of water and low temperatures. Investigations were conducted for a randomly selected aggregate sample of 8-16 mm fraction and rock taken directly from the excavations, which corresponded to aggregate grains in colour and texture.

As indicated in the introduction, aggregate usability for frost resistance concretes is, to a large extent, determined by its porosity, absorbability, size and geometrical arrangement of pores, therefore investigations focused on the assessment of those features changeability, both in the aggregate and the corresponding rock material.

As regards changes in colour and texture, due to macroscopic assessment of the aggregate and rock samples, it was possible to identify 4 groups of the material, whose colour and texture were similar. For each group, absorbability, specific density, volumetric density, porosity, freeze/thaw resistance, pore size distribution investigations were conducted. Freeze/thaw resistance investigations of aggregate grains and rock samples were carried with direct freeze/thaw test method (25 cycles of freezing in air and thawing in

water), whereas pore size distribution was examined with mercury porosimetry method.

3. Description of investigations and results obtained

The aggregate under consideration originates in calcareous rocks, light to dark grey in hue and of much diversified texture. Macroscopic examination of the aggregate and rock samples revealed considerable heterogeneity of the aggregate and rock grains, caused by significant diversification of the stratum in operation. An overall view of the aggregate sample is shown in Fig. 1, whereas in Fig. 2 one can see the view of grains similar in hue and texture, identified in the sample assessed, together with their mass fraction in the whole sample.

Fig. 1. Overall view of aggregate sample

Grains making up the aggregate and the corresponding rock material were divided into 4 groups marked by letters A, B, C and D. A-marked grains, which came from porous limestone, light grey in hue with rough fracture, constituted 64% of the sample mass. B-marked grains, which originated in broken limestone, were similar in light grey hue to A-marked grains, but with smooth vitreous fracture. Those constituted 15% of the sample mass. C- and D-marked grains came from broken limestone with smooth vitreous fracture, grey (C-marked grains) or dark grey in hue with numerous calcite crystals (D-marked grains). Their mass fractions in the total aggregate mass amounted to 12% and 9% for C- and D-marked grains, respectively.

Fig. 2. View of aggregate sample after grouping grains of similar hue and texture, mass fraction of each group in the sample is provided

Table 1 presents physical properties of the rock material from the deposit assessed.

Macroscopically, examined rock samples corresponded to aggregate grains marked A, B,

Table 1. Physical properties of the aggregate and rock material

Item	Examined property	Examination result			
		A	B	C	D
1	Density, g/cm^3 *	2.68			
2	Volumetric density, g/cm^3	2.36	2.40	2.56	2.60
3	Porosity, %	11.9	10.4	4.5	3.0
4	Mass absorbability, %	4.5	4.2	1.9	1.1
5	Direct freeze/thaw resistance of: - rock, - aggregate	cracks no cracks	cracks no cracks	cracks cracks	no cracks no cracks

* the rock specific density was determined for averaged material sample in accordance with the Polish standard PN-76/B-06714

C and D. In spite of macroscopic differences, A- and B-marked rocks were characterised by low volumetric density (approx. 2.36-2.40 g/cm³), high porosity (above 11%) and high absorbability (above 4%), and also low freeze/thaw resistance (Fig. 3). Aggregate grains originating in those rocks, however, did not demonstrate damages due to freeze/thaw resistance tests (Fig. 4). The C-marked rock had low porosity and absorbability (approx. 2%), as well as insufficient freeze/thaw resistance, which resulted in visible cracking of frozen/thawed rock samples (Fig. 5) and crumbling of aggregate grains (Fig. 6). The D-marked rock sample was characterised by good resistance to freezing/thawing cycles (no cracks or crumbling were noted), although its porosity and absorbability were similar to those in C-marked rock. Such behaviour was demonstrated by both rock samples and aggregate grains.

Fig. 3. Crack in A-marked rock sample caused by freeze/thaw resistance tests

Fig. 4. View of aggregate sample from A-marked rock following freeze/thaw resistance tests
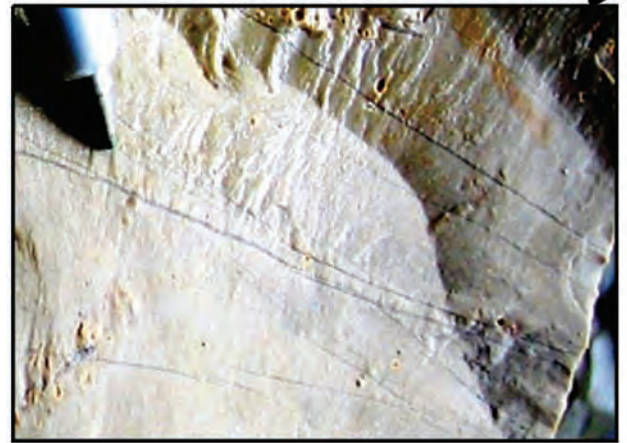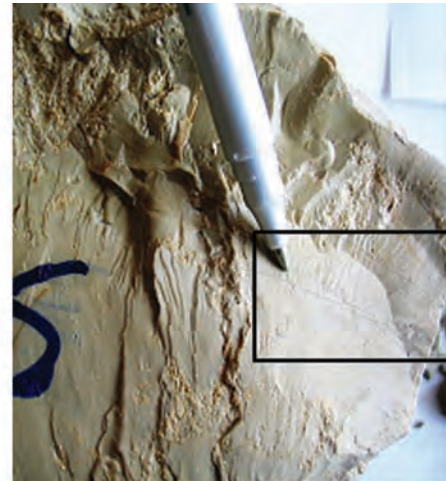

Fig. 5. Crack in C-marked rock sample

Fig. 6. View of C-marked aggregate sample following freeze/thaw resistance tests

Aggregate freeze/thaw resistance depends, to a large extent, on the distribution of pore sizes inside aggregate grains. This opinion was followed in the F

annexe titled "Guidelines for Aggregate Freeze/Thaw Resistance Assessment" to the Polish standard PN EN 12620:2004 "Aggregates for Concrete".

In order to determine pore size distribution in aggregate grains mercury porosimetry investigations into aggregate grains from A, B, C and D-marked rocks were conducted. The results of pore size distribution investigations are presented, in the form of integral curves, in Figs. 7-10.
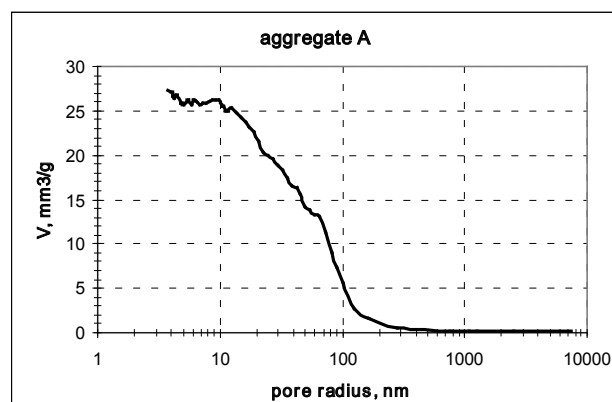

Fig. 7. Pore size distribution in aggregate from A-marked rock
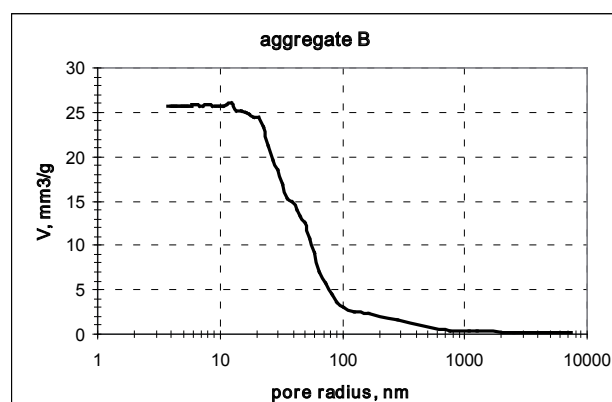

Fig. 8. Pore size distribution in aggregate from B-marked rock
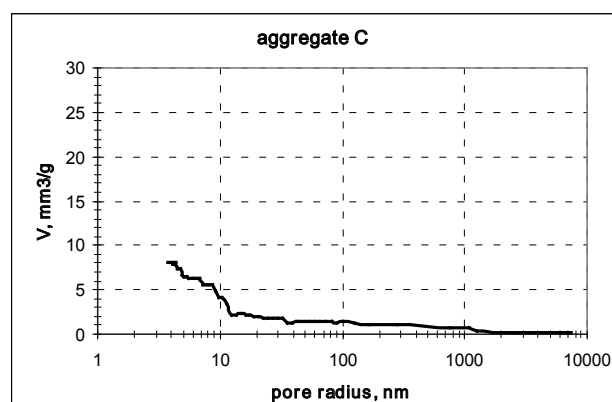

Fig. 9. Pore size distribution in aggregate from C-marked rock
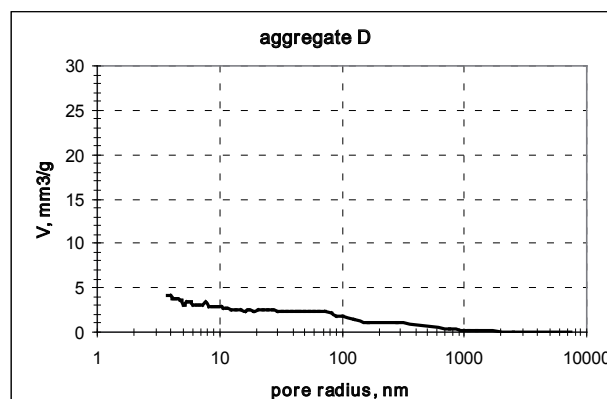
Fig. 10. Pore size distribution in aggregate from D-marked rock

On the basis of pore size distribution curves in Figs. 1-4, it can be observed that aggregates from A- and B-marked rocks (Figs. 7 and 8) are characterised by similar total porosity and high content of pores that range 10-100 nm in radius, which may be the reason for damages to concrete exposed to the action of water and low temperatures. With respect to concrete freeze/thaw resistance, aggregate capillary pores of radiuses ranging 5-100 nm are thought to be detrimental. Such pores are easily filled with water, which when frozen, exerts hydraulic pressure on the inside of grain thus causing its damage, as well as damage to the surrounding paste [1], [3]. Total porosity in the aggregate from C-marked rock (Fig. 9) is almost three times lower when compared with aggregates A and B, yet both its rock samples and aggregate grains were damaged in direct freeze/thaw resistance tests. The reason for that is a high content of small pores of less than 10 nm radius, as well as their proportion to larger pores. Water in pores of radius as above is strongly affected by surface phenomena, which increases hydraulic resistances in flow and causes considerable increase in pressure inside grain when it is frozen due to quick temperature drop. On the other hand, the aggregate from D-marked rock (Fig. 10) stands out due to the lowest total porosity and proportional distribution of pore sizes in the whole range examined. That indicates advantageous properties of aggregate obtained from a rock of this kind as regards concrete freeze/thaw resistance.

4. Conclusions

In addition to granulometric features of aggregate, they are physical and mechanical properties of rock material from which it is produced, that decide

about its usability for construction industry and, in particular, concrete technologies. Granulometric features such as graining, grain shapes, the content of over- and under-grain, or finally impurities content can be modified in the course of aggregate production due to the application of appropriate technological solutions. Physical and mechanical properties of rock material, however, were determined by nature and differ for various quarrying sites and even within the same stratum.

The calcareous aggregate being assessed is characterised by high changeability of physical properties. The examined sample was composed of grains originating in 4 kinds of calcareous rocks. Those of their properties which are important for the durability of concrete exposed to the action of water and low temperatures were highly diversified. Therefore, it is very probable that freeze/thaw resistance of concrete produced with such aggregate will vary greatly, depending on proportions of different rock kinds in the aggregate composition. Furthermore, when such aggregate is used to produce cement concrete, differences in consistency or

strength of the concrete can occur, which also affects its durability. The significance of this phenomenon grows with a higher class of concrete produced.

As the demand for concrete aggregate grows, it is expected that the use of aggregate from calcareous rocks for the production of concretes exposed to harsh operational conditions will tend to increase. In order to ensure high durability of concrete with such aggregates, in addition to the choice of material of proper physical properties, it is also necessary to account for their retaining stability through time.

References

[1] Rusin Z.; *Technology of Frostproof Concretes (in Polish)*; Polski Cement Ltd; Cracow 2002

[2] Stelmaszczyk G.; *Assessment of Water Phase Change in Aggregate with Respect to its Usability for Frostproof Concretes (in Polish)*; doctoral theses; Kielce 1999

[3] Rusin Z., Wawrzeńczyk J., Stelmaszczyk G.; *Extension of Aggregate Classification Methods for Bridge, Hydrotechnical and Surface Concretes (in Polish)*; KBN research project no 7 7227 92 03; Kielce 1995

Grzegorz Stelmaszczyk
Przemysław Świercz

Ocena przydatności kruszywa wapiennego do betonów mrozoodpornych

1. Wstęp

O przydatności kruszywa do betonów mrozoodpornych decydują jego właściwości fizyczne, a w szczególności porowatość, nasiąkliwość czy wielkość i układ geometryczny porów [1], [2]. Z praktycznego punktu widzenia istotna jest również stabilność tych parametrów dla poszczególnych partii kruszywa. Warunek ten jest często trudny do spełnienia w przypadku kopalni eksploatujących złoża uwarstwione, o różnym pochodzeniu i różnych właściwościach fizycznych. W szczególności dotyczy to skał wapiennych.

2. Metodyka badań i uzyskane wyniki

Oceniane kruszywo pochodziło ze skał wapiennych o barwie od jasno do ciemnoszarej i mocno zróżnicowanej teksturze. Na podstawie makroskopowych oględzin kruszywa i próbek skały stwierdzono znacz-

ną niejednorodność ziaren kruszywa i skały, spowodowaną zróżnicowaniem eksploatowanego pokładu. Na rys. 1 przedstawiono widok wyodrębnionych, z ocenianej próbki, ziaren o zbliżonej barwie i teksturze wraz z ich udziałem wagowym w całej próbie.

Wchodzące w skład kruszywa ziarna oraz odpowiadający im surowiec skalny podzielono na 4 grupy oznaczone literami A, B, C i D. Ziarna oznaczone literą A stanowiły ziarna porowatego wapienia o jasnoszarej barwie i szorstkim przełomie, stanowiące 64% masy próby, literą B oznaczono ziarna ze zbitego wapienia o zbliżonej do ziaren A jasnoszarej barwie, lecz gładkim, szklistym przełomie, stanowiące 15% masy próbki. Ziarna oznaczone literami C i D stanowiły ziarna zbitego wapienia o gładkim szklistym przełomie, barwie szarej (ziarna C) lub ciemnoszarej z licznymi kryształami kal-

cytu (ziarna D). Ich udział w całkowitej masie kruszywa wynosił odpowiednio 12% dla ziaren C i 9% w przypadku ziaren D.

Mrozoodporność kruszywa zależy w dużej mierze od rozkładu wielkości porów wewnątrz ziaren kruszywa. Pogląd ten znalazł się w załączniku informacyjnym F zatytułowanym „Wskazówki dotyczące oceny mrozoodporności kruszywa" normy PN EN 12620:2004 „Kruszywa do betonu". W celu określenia rozkładu wielkości porów w ziarnach kruszywa wykonano badania metodą porozymetrii rtęciowej ziaren kruszywa ze skał A, B, C i D.

Z przeprowadzonych badań rozkładu wielkości porów wynika, że kruszywa ze skał oznaczonych literami A i B mają zbliżoną porowatością całkowitą i dużą zawartością porów o promieniach z przedziału 10-100 nm. co może być przyczyną uszkodzeń betonu narażonego na działanie wody i ujemnych temperatur. Poddane bezpośredniemu zamrażaniu próbki skały A i B uległy uszkodzeniu. Porowatość całkowita kruszywa ze skały oznaczonej literą C jest ponad trzykrotnie mniejsza w porównaniu do kruszyw A i B, jednak zarówno próbki skały jak i ziarna kruszywa uległy uszkodzeniu w badaniu mrozoodporności bezpośredniej. Przyczyną tego jest duża zawartość porów drobnych o promieniach poniżej 10 nm oraz ich proporcje w stosunku do porów większych. Woda w porach o takich promieniach podlega silnym oddziaływaniom powierzchniowym, co zwiększa opory hydrauliczne przepływu i powoduje znaczny wzrost ciśnienia wewnątrz ziarna podczas zamrażania [2]. Kruszywo ze skały oznaczonej literą D wyróżnia się najniższą porowatością całkowitą i proporcjonalnym rozkładem wielkości porów w całym badanym zakresie. Wskazuje to na korzystne z punktu widzenia mrozoodporności betonu właściwości kruszywa pozyskanego z tego rodzaju skały.

3. Podsumowanie

Oceniane kruszywo wapienne cechuje się znaczną zmiennością właściwości fizycznych. Analizowana próbka złożona była z ziaren pochodzących z 4 rodzajów skał wapiennych o mocno zróżnicowanych właściwościach, istotnych z punktu widzenia trwałości betonu narażonego na działanie wody i niskich temperatur. Istnieje zatem wysokie prawdopodobieństwo znacznej zmienności mrozoodporności betonu wykonanego z tego rodzaju kruszywem w zależności od wzajemnych proporcji poszczególnych rodzajów skały w stosie okruchowym. Ponadto w przypadku wykorzystania tego rodzaju kruszywa do produkcji betonu cementowego mogą wystąpić różnice w konsystencji czy wytrzymałości produkowanego betonu, co również nie pozostaje bez wpływu na jego trwałość. Znaczenie tego zjawiska rośnie wraz ze wzrostem klasy produkowanego betonu.

W związku ze wzrostem zapotrzebowania na kruszywo do betonu, należy spodziewać się coraz szerszego wykorzystania kruszyw ze skał wapiennych do produkcji betonów narażonych na trudne warunki eksploatacyjne. Dla zapewnienia wysokiej trwałości betonu z tego rodzaju kruszywami należy, oprócz wyboru surowca o odpowiednich właściwościach fizycznych, zwrócić również uwagę na zachowanie ich stabilności w czasie.

PAWEŁ KOSSAKOWSKI

Kielce University of Technology,
Al. Tysiąclecia Państwa Polskiego 7,
25-314 Kielce, Poland,
e-mail: kossak@tu.kielce.pl

APPLICATION OF THE ACOUSTIC EMISSION METHOD IN ORDER TO DETERMINE THE CRACK INITIATION MOMENT IN TIMBER

Abstract

Wooden structural elements frequently develop cracks, which can be dangerous if the elements are under service conditions. Cracks usually propagate parallel to the element axis, and their depth of several centimeters is frequently the same as the thickness of the element. Almost all timber cracks are classified as serious defects. They are responsible for lower strength parameters and lower biocorrosion resistance.

The acoustic emission (AE) method, which is commonly used for testing objects or structures made of steel or reinforced concrete, can now be applied to analyze the fracture toughness of timber structures and then diagnose and monitor their safety. This refers to both statically and dynamically loaded elements, e.g. timber support structures in mine galleries.

Keywords: acoustic emission, crack in timber, crack initiation

1. Introduction

An example of wooden cracks is presented in Fig. 1.

Fig. 1. View of the cracks in the angle brace, the purlin and the rafter

The load capacity of an element with a crack is dependent on the element fracture toughness. It is determined in accordance with the principles of fracture mechanics.

The following parameters are used for timber: the critical energy release rate $G_{\alpha c}$, and the critical stress intensity factor $K_{\alpha c}$, where α denotes the loading mode (I, II or III). The first case ($\alpha =$ I) is the cleavage. It is also called the crack opening. Cleverage occurs when the load is applied normal to the crack plane. The second case is the in-plane shear ($\alpha =$ II). It occurs, when the load is applied parallel to the crack and acts normal to the crack edge. The third case, the so-called out-of-plane shear ($\alpha =$ III). It occurs when the load is in the crack plane but it is parallel to the crack edge.
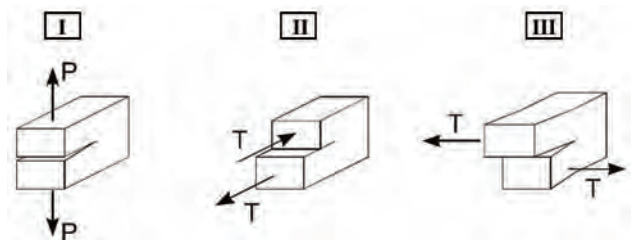
Fig. 2. Three basic loading modes of an element with a crack: mode I – cleavage, mode II – in-plane shear, mode III – out-of-plane shear

The fracture toughness of a material is determined by measuring the critical load, P_c. This corresponds to the moment of crack initiation. It is essential to analyze the phenomenon of crack initiation, because it has a direct effect on the values of $G_{\alpha c}$ and $K_{\alpha c}$. It is important to apply the method which is justified, simple and precise.

2. The methods used for determining the moment of crack initiation in timber

Timber is regarded as anisotropic material. The crack initiation moment and the value of the critical load, P_c, can be determined with various methods and

standards. The most common techniques discussed in Refs. [1] and [2] are shown in Fig. 3. The first one is the non-linearity (*NL*) method. It is based on a change in the element compliance. The crack initiation moment coincides with the non-linearity point on the load-displacement (*P-δ*) curve. This point corresponds to the value of the critical load $P_{c(NL)}$. In practice, it is impossible to determine this point precisely.

Fig. 3. Methods used for determining the critical load P_c

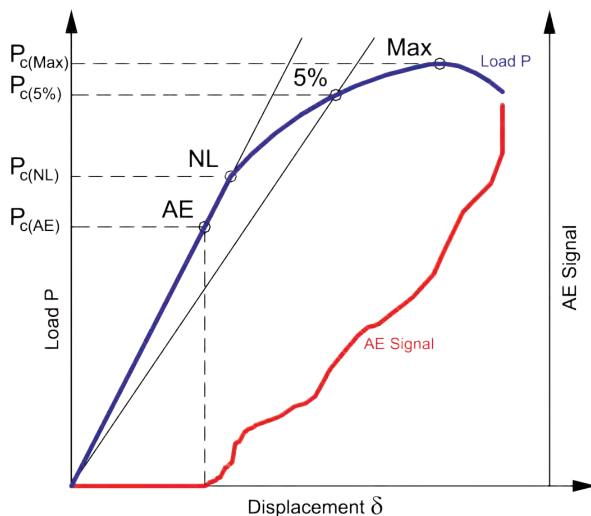The second method assumes that the crack initiation moment coincides with the point of intersection of the *P-δ* curve with a straight line. The tangent of slope is 5% less as compared to slope of the straight line with a linear section of the *P-δ* curve. This method was originally derived for metals. It assumes that in the case of a slowly propagating crack, the critical load corresponds to a 2% increase in the crack length. It is important to consider the deviation of the *P-δ* curve from the straight line with a linear section resulting from the plastic strain. This increases the departure from the linear part of the curve by additional 2%. The influence of the specimen geometry causes a deviation from linearity by 1%. A change in the specimen geometry results in a deviation from the straight line with the linear section of the *P-δ* curve and is assumed to be 5%. The load corresponding to the point designated as 5% is assumed to be the critical load $P_{c(5\%)}$. This method is also suitable for composites. The critical load is frequently assumed to be the same as the maximum value of the force applied in a test. This corresponds to the point designated as *Max*. In this case, the value of the critical load corresponds to $P_{c(Max)}$.

For timber, however, the approach based on the acoustic emission (*AE*) method seems to be the most

suitable [3-8]. The load at which acoustic signals occur is assumed to be the crack initiation moment. The value of the critical load $P_{c(AE)}$ corresponds to the *AE* point shown in Fig. 3 [2].

3. The Acoustic Emission (*AE*) method

The numerous applications of the *AE* method include: testing materials and their strength, monitoring the safety of structural elements and whole buildings, testing the tightness of elements of engineering systems, geological and seismic tests, and finally, detecting and locating discharges in high-voltage transformers. Crack initiation is accompanied by the emission of acoustic impulses. The acoustic emission method is one of few non-destructive method. It can be used to detect a defect propagating in a solid which is subjected to load. One of the main advantages of the *AE* method over the traditional methods of engineering control is that it permits detecting early changes in the material microstructure. It also allows monitoring the slowly propagating defects in elements of engineering structures on the basis of acoustic signals.

An acoustic emission signal is generated by a change in the energetic state of the material or release of its internal energy. If the material with stored inner energy is subjected to an external stimulus, or the material state changes, then the state of its energy stored will change as well, and part of it will be released. The released energy is used to produce mechanical work or heat. Only a relatively small part of this energy is converted to elastic waves in the form of acoustic emission signals. An *AE* signal generated in the volume of the material as elastic waves reaches the material surface. This can be registered with receiving instrument. An *AE* signal contains lots of information. Most of it, however does not characterize the sources or the existing phenomena. An analysis of the acoustic signal can be done with the choice of selected parameters (Fig. 4). The most important of them are:
- the number of *AE* events, i.e. the number of envelopes of *AE* impulses for which the amplitude exceeds a certain arbitrarily selected level of reference or level of discrimination;
- the number of *AE* counts, i.e. the number of areas for which the amplitude exceeds the level of discrimination.

The form of a single *AE* impulse and some of its parameters are shown in Fig. 4.
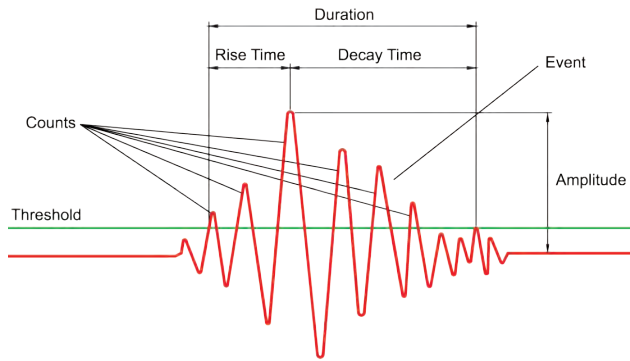
Fig. 4. Parameters characterising an acoustic impulse

The level of discrimination has little influence on the value of the sum of counts. This implies good correlation with the actual number of *AE* events [9]. The number of *AE* counts is an important parameter frequently used in practice.

4. Applying the *AE* method to detect the crack initiation moment in timber

The crack initiation moment and the critical load P_c of timber elements under analysis were determined with the *AE*, *NL*, 5% and *Max* methods.

The tests were conducted for pinewood specimens (*Pinus silvestris*) modeling beam timber elements. *TL* stands for the load applied tangentially and *RL* stands for the load applied radially, with respect to arrangement of fibers and growth rings. *L*, *T*, and *R* stand for the longitudinal, tangential, and radial directions, respectively. Two types of specimens (*B* x *2h* = 18x18 mm), were used for modeling the beam elements with longitudinal cracks. The *DCB* (*Double Cantilever Beam*) specimens were subjected to cleavage (α = I, Fig. 5a) and the *ENF* (*End Notched Flexure*) specimens, which were subjected to longitudinal shear (α = II, Fig. 5b).

The facility for testing consisted of a strength testing machine, a strain-gauge bridge, an acoustic emission processor and a PC with an analog-digital card. All measurements were conducted with strength testing machine (UTS System 209) with a load capacity of 20 kN. During strength tests were measured: load *P*, displacement δ of the point of application of force, and an acoustic emission signal. The *AE* signals were registered with *AE* system processor 204A, made by Acoustic Emission Technology Corp. (USA). *AE* signals were measured using a resonance sensor with a frequency of 175 kHz coupled to an *AE* signal preamplifier. The sensor was mounted on the side surface of the specimens, just behind the crack tip

(Fig. 5a and b). After a signal was amplified, the number of *AE* counts was registered. During the strength tests, the force for which acoustic emission signals appeared was assumed to be the critical load, P_c, [i.e. the load under which a crack was initiated].
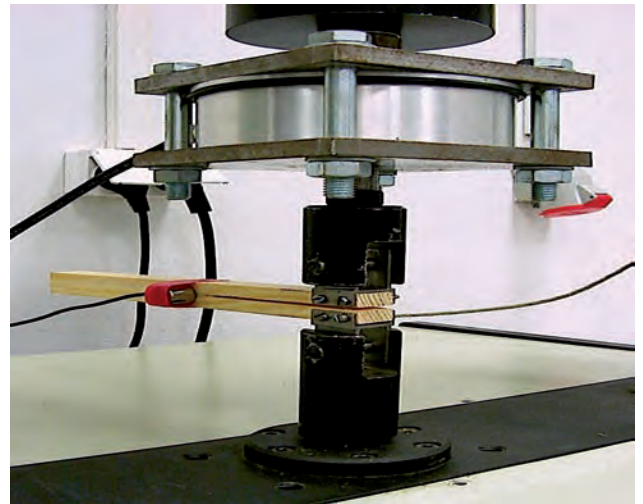
a)
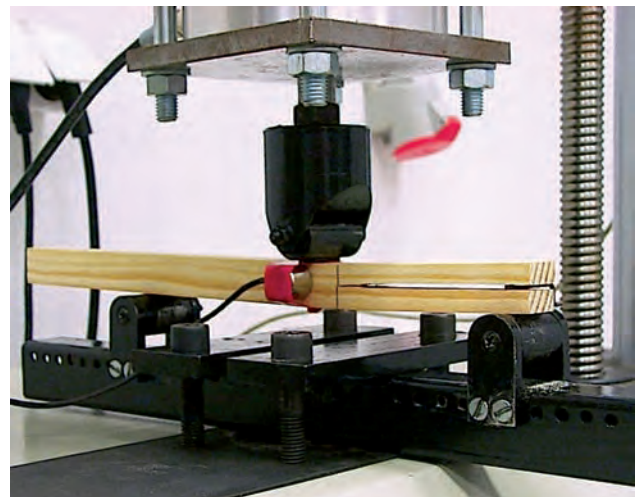
b)

Fig. 5. Specimens under test: a) *DCB* (α = I loading mode); b) *ENF* (α = II loading mode)

For loading modes I and II (Fig. 6a, b), there is the relation between the values of the critical load determined with the *AE*, *NL*, 5% and *Max* methods: $P_{c\,(AE)} < P_{c\,(NL)} < P_{c\,(5\%)} < P_{c\,(Max)}$. The difference between $P_{c\,(AE)}$ and $P_{c\,(NL)}$ is 4% and between $P_{c\,(AE)}$ and $P_{c\,(5\%)}$ 8%
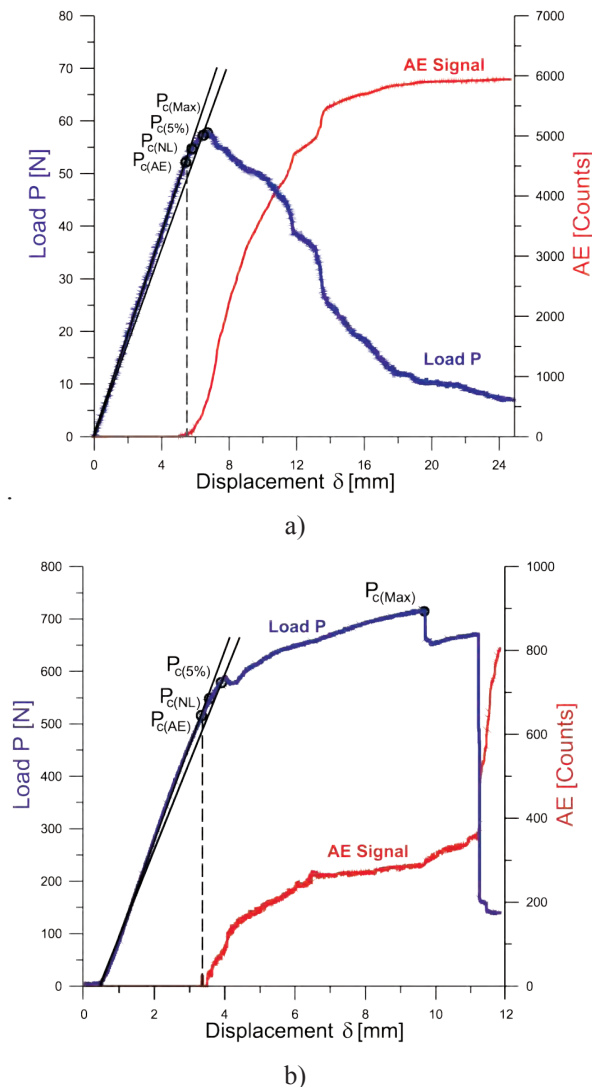
a)

b)

Fig. 6. Determining P_c for pinewood: a) the *DCB* specimen (α = I); b) the *ENF* specimen (α = II)

As can be seen (Fig. 6. above) the choice of the method to determinine the crack initiation moment is very important. This affects the value of the factor defining the fracture toughness ($K_{\alpha c}$, $G_{\alpha c}$). The 5% and *Max* methods cause that the value of P_c is too high, and so is the value of fracture toughness. If we assume that $P_c = P_{c(Max)}$ the critical values of $G_{\alpha c}$ are 8% and as much as 38% higher for loading modes I and II, respectively, than the values of $G_{\alpha c}$ determined with the *AE* method. In the case of non-uniform materials, the 5% and *Max* methods are not justified. Therefore their application to timber analysis is limited.

The *AE* and *NL* methods are justifiable. In the case of the *NL* method it is the change in the element compliance that is related to the critical value of $G_{\alpha c}$. The load values obtained using the two methods are similar. This implies, that the crack initiation moment can be determined with either one. Determining the exact non-linearity point in the *NL* method may be difficult because its value is always subjective. The value of the corresponding load is also a certain approximation. When the *AE* method is applied, no such difficulties or uncertainties are reported. This method seems to be optimal for numerous reasons. It can be used for analyzing the fracture dynamics of timber, determining the crack initiation moment, and, accordingly, determining the fracture toughness of this material. Determining the crack initiation moment based on the analysis of acoustic signals is not complicated. The measurement procedure is simple.

6. Conclusion

The acoustic emission (*AE*) method, which is commonly used for testing objects or structures made of steel or reinforced concrete, can also be applied to analyze the fracture toughness of timber structures and to diagnose and monitor their safety. This refers to both statically and dynamically loaded elements, e.g. timber support structures in mine galleries. By applying the *AE* method one is able to determine the moment of crack initiation, and accordingly, the moment of failure.

References

[1] Davies P.: *Protocols for Interlaminar Fracture Testing of Composites*, European Structural Integrity Society Polymers & Composites Task Group, 1992.

[2] Ducept F.: Davies P., Gamby D., *An Experimental Study to Validate Tests Used to Determine Mixed Mode Failure Criteria of Glass/Epoxy Composites*, Composites Part A, Vol. 28A, pp. 719-729, 1997.

[3] Sato K., Honda T., Fushitani M.: *Fracture Toughness and Acoustic Emission of Wood*, Progress in Acoustic Emission III, The Japanese Society of NDI, pp. 602-608, 1986.

[4] Kossakowski P.: *Fracture Toughness of Wood,* 2nd International Conference, Fracture Mechanics of Materials and Structural Integrity, Lviv, pp. 241-246, 1999.

[5] Kossakowski P.: *Analiza odporności na pękanie drewna,* VII Krajowa Konferencja Mechaniki Pękania, Kielce/Cedzyna, s. 241-248, 1999.

[6] Reiterer A., Stanzl-Tschegg S.E.: Tschegg E.K.: *Mode I Fracture and Acoustic Emission of Softwood and Hardwood*, Wood Science and Technology, Vol. 34, pp. 417-430, 2000.

[7] Raczkowski J., Moliński W., Ranachowski Z.: *Acoustic Emission in Fracture Mechanics of Wood,* Journal of Theoretical and Apllied Mechanics, Vol. 32, pp. 301-322, 1994.

[8] Moliński W.: *Detekcja powstawania i rozwoju pęknięć w drewnie przy użyciu metody emisji akustycznej (EA),*

Roczniki Akademii Rolniczej w Poznaniu, Rozprawy Naukowe, Zeszyt 288, Poznań 1998.

[9] Malecki I., Ranachowski J.: *Emisja akustyczna. Źródła, metody, zastosowania.* Praca zbiorowa, Wydawnictwo IPPT PAN, Warszawa, 1994.

Paweł Kossakowski

Zastosowanie emisji akustycznej do wyznaczania inicjacji pękania drewna

1. Wprowadzenie

Pękanie jest zjawiskiem często występującym w drewnianych elementach konstrukcji budowlanych. O nośności elementu zawierającego pęknięcie decyduje odporność na pękanie, określana zgodnie z zasadami mechaniki pękania, za pomocą jednego z kilku parametrów. W przypadku drewna są to krytyczne wartości współczynnika uwalniania energii $G_{\alpha c}$ oraz współczynnika intensywności naprężeń $K_{\alpha c}$ (α = I, II, III oznacza sposób obciążenia). Podstawową wielkością mierzoną przy wyznaczaniu odporności na pękanie, jest tzw. obciążenie krytyczne P_c. Obciążenie to odpowiada momentowi inicjacji procesu pękania materiału oraz bezpośrednio wpływa na wielkość $G_{\alpha c}$ i $K_{\alpha c}$ (rys. 3).

Spośród obecnie stosowanych metod wyznaczania obciążenia krytycznego [1, 2] należy wymienić metodę spadku podatności *NL*, obciążenia maksymalnego *Max* i metodę 5% (rys. 3). Jak wykazano poniżej, w odniesieniu do drewna najbardziej uzasadnione wydaje się być podejście bazujące na metodzie emisji akustycznej *EA*. Jest to jedna z niewielu metod nieniszczących pozwalających wykryć wady, które w ciele stałym poddanym obciążeniu rozwijają się, powstawaniu pęknięcia towarzyszy emisja impulsu akustycznego. Za moment inicjacji pękania drewna przyjmowane jest obciążenie, przy którym pojawiają się sygnały akustyczne. Wartość obciążenia krytycznego $P_{c(EA)}$ odpowiada punktowi oznaczonemu na rys. 3 jako *EA*. Poniżej przedstawiono wyniki badań dotyczących wyznaczania obciążenia krytycznego P_c elementów drewnianych przy zastosowaniu metody emisji akustycznej *EA* oraz metod *NL* i 5%.

2. Detekcja inicjacji pękania drewna za pomocą emisji akustycznej EA

Badania przeprowadzono na próbkach modelujących drewniane elementy belkowe z drewna sosnowego (*Pinus silvestris*) z pęknięciami podłużnymi względem włókien. Użyto próbek o przekroju 18x18 mm dwóch typów: *DCB (Double Cantilever Beam)*, próbki rozrywane (α = I sposób obciążenia) i *ENF (End Notched Flexure)* próbki poddane ścinaniu wzdłużnemu (α = II sposób obciążenia). Podczas prób wytrzymałościowych rejestrowano obciążenie *P*, przemieszczenie δ oraz ilość zliczeń *EA (counts)*. Czujnik *EA* umieszczany był na bocznej powierzchni próbek, bezpośrednio za wierzchołkiem pęknięcia.

Dla obydwu analizowanych sposobów obciążenia (rys. 6a, b) pomiędzy wartościami obciążenia krytycznego wyznaczonymi na podstawie metod *NL*, 5% i *EA* zachodzi relacja $P_{c\,(EA)} < P_{c\,(NL)} < P_{c\,(5\%)}$. Różnice w wielkości obciążeń wynoszą 4% pomiędzy $P_{c\,(EA)}$ i $P_{c\,(NL)}$ oraz 8% pomiędzy $P_{c\,(EA)}$ i $P_{c\,(5\%)}$.

Analizując uzyskane wyniki należy stwierdzić, że zastosowanie metody 5% i obciążenia maksymalnego powoduje zawyżanie wartości P_c, co bezpośrednio przekłada się na odporność na pękanie drewna. W przypadku przyjęcia $P_c = P_{c(Max)}$ krytyczne wartości $G_{\alpha c}$ są o 8% i 38% wyższe odpowiednio dla I i II sposobu obciążenia w porównaniu do wartości $G_{\alpha c}$ wyznaczonych przy użyciu metody *EA*. Uwzględniając również, że metody 5% i obciążenia maksymalnego nie mają fizycznego uzasadnienia w odniesieniu do materiałów niejednorodnych,

ich zastosowanie w analizie pękania drewna jest ograniczone.

Metody *EA* i *NL* są fizycznie uzasadnione (w przypadku metody *NL* jest to spadek podatności elementu), a uzyskane wartości P_c są do siebie zbliżone. Niestety dokładne ustalenie punktu nieliniowości *NL* może nastręczać pewne trudności i jest zawsze subiektywne, a wartość obciążenia jemu odpowiadającego $P_{c(NL)}$ jest pewnym przybliżeniem. Zastosowanie metody emisji akustycznej *EA* nie nastręcza takich trudności i niejasności, dlatego też metoda ta wydaje się być z wielu względów optymalną. Umożliwia ona analizę dynamiki procesu pękania drewna, pozwala na ścisłe ustalenie momentu inicjacji procesu pękania oraz odpowiadającego mu obciążenia krytycznego P_c. Analiza sygnału akustycznego *EA* nie jest zbyt skomplikowana, a pomiar nie nastręcza w zasadzie żadnych trudności.

3. Podsumowanie

Metoda emisji akustycznej *EA*, która jest coraz powszechniej stosowana w badaniach obiektów i konstrukcji wykonanych ze stali czy żelbetu, może z powodzeniem znaleźć zastosowanie w badaniach odporności na pękanie drewna jak również diagnostyce i monitoringu bezpieczeństwa pracy konstrukcji drewnianych. Dzięki zastosowaniu metody *EA* możliwe jest natychmiastowe wykrycie inicjacji pękania drewna informując użytkownika o nadchodzącym zagrożeniu – możliwości zniszczenia konstrukcji.

JOZEF MELCER

University of Žilina, Faculty of Civil Engineering,
Department of Structural Mechanics,
Komenského 52, 010 26 Žilina, Slovak Republic,
e-mail: jozef.melcer@fstav.uniza.sk

DYNAMIC DEFLECTIONS OF BRIDGES DUE TO MOVING LOAD

A b s t r a c t

The problem of vehicle-bridge interaction can be followed in the literature from the year 1849. It was induced by the collapse of the Chester Rail Bridge in England in the year 1847. At the early stage the analytical methods were applied. The development of computers brings the change in the approach to the used methods of solution. The Finite Element Methods and the Component Element Methods represent the revolution and qualitative jump in the development. The dynamic deflections and the values of dynamic coefficients are remarkable from the point of bridge designers. The analysis of dynamic coefficients on the frequency ratio of natural frequency of vehicle and natural frequency of a bridge and dependence of dynamic coefficients on the speed of vehicle motion are presented in this contribution.

Keywords: dynamics, vehicle – bridge interaction, computing model, numerical solution.

1. Introduction

The problem of vehicle-bridge interaction can be followed in the literature from the year 1849. It was induced by the collapse of the Chester Rail Bridge in England in the year 1847 [1]. While the problem of dynamic of railway bridges was followed from the year 1847 the problems of dynamic of highway bridges start to be followed in the 20th century only. The 1st important report on this topic was published by the American Society of Civil Engineers [2]. Total review about results of solution to the year 1975 was published by Tseng Huang in [3]. Also in the Czech and Slovak Republic important works arose in this field. In the area of railway bridges they were published by Frýba, L. [4] and in the area of highway bridges they were published by Melcer, J. [5]. Numerical modeling of the vehicle motion along bridge structure requires paying attention minimally to these facts: creation of computing models of vehicles, creation of computing models of bridges, creation of computing programs for the solution of the equations of motion and displaying of obtained results.

2. Computing models of vehicles

The discrete computing models of vehicles can be created on three qualitative different levels: 1D – quarter model, 2D – plane model and 3D – space model. Every model has its advantages and disadvantages and under certain assumptions it can be used for the solution

of real practical problems. Possible plane computing models of a lorry and a bus are shown in the Fig. 1. The relation between the components of displacements $\{\mathbf{r}(t)\}$, corresponding to individual degrees of freedom, and deformations of jointing members $\{\mathbf{d}(t)\}$ gets the transpose static matrix $[\mathbf{A}]^{\mathrm{T}}$

$$\{\mathrm{d}(\boldsymbol{t})\} = [\mathrm{A}]^{\mathrm{T}} \cdot \{\mathrm{r}(\boldsymbol{t})\} \tag{1}$$

Dependence between elastic forces in jointing members (in the sense of action of mass objects on jointing members) and its deformations is described by the equation

$$\{\mathbf{F}_{\mathrm{re}}(t)\} = [\mathbf{k}] \cdot \{\mathbf{d}(t)\} \tag{2}$$

where $[\mathbf{k}]$ is the stiffness matrix of jointing members. Dependence of damping forces on the velocity of deformations $\{\dot{\mathbf{d}}(t)\}$ is described by the equation

$$\{\mathbf{F}_{\mathrm{d}}(t)\} = [\mathbf{b}] \cdot \{\dot{\mathbf{d}}(t)\} \tag{3}$$

where $[\mathbf{b}]$ is damping matrix. By dot is denoted derivation with respect of time t. Friction forces are considered as

$$\text{if } \{\dot{\mathbf{d}}(t)\} \geq + \dot{d}_c \qquad \{\mathbf{F}_{\mathrm{f}}(t)\} = + \{\mathbf{f}\} \, ,$$

$$\text{if } \{\dot{\mathbf{d}}(t)\} \leq - \dot{d}_c \qquad \{\mathbf{F}_{\mathrm{f}}(t)\} = - \{\mathbf{f}\} \, , \tag{4}$$

$$\text{if abs}\{\dot{\mathbf{d}}(t)\} < \dot{d}_c \qquad \{\mathbf{F}_{\mathrm{f}}(t)\} = + \{\mathbf{f}\}^{\mathrm{T}} \cdot \{\dot{\mathbf{d}}(t)\} / \dot{d}_c \, .$$

Resulting forces in jointing members in action on mass objects are

$$\{F_{SC}(t)\} = - \{F_{re}(t)\} - \{F_d(t)\} - \{F_f(t)\} . \qquad (5)$$

Sign (-) is due to the principle of action and reaction. From the forces in jointing members $\{F_{SC}(t)\}$ the static equivalents corresponding to individual degrees of freedom $\{F_{SV}(t)\}$ are calculated

$$\{F_{SV}(t)\} = [A] . \{F_{SC}(t)\} . \qquad (6)$$

To the forces corresponding to individual degrees of freedom $\{F_{SV}(t)\}$ the gravity forces $\{F_G\}$ and reactions in support $\{F_{RV}(t)\}$ must be added. In this manner we obtain the complete vector of forces $\{F_V(t)\}$ acting on the computing model of vehicle

$$\{F_V(t)\} = \{F_{SV}(t)\} + \{F_G\} + \{F_{RV}(t)\} . \qquad (7)$$

The system of equations of motion describing the vibration of the computing model of vehicle is then expressed by the relation

$$[m] . \{\ddot{r}(t)\} = \{F_V(t)\} , \qquad (8)$$
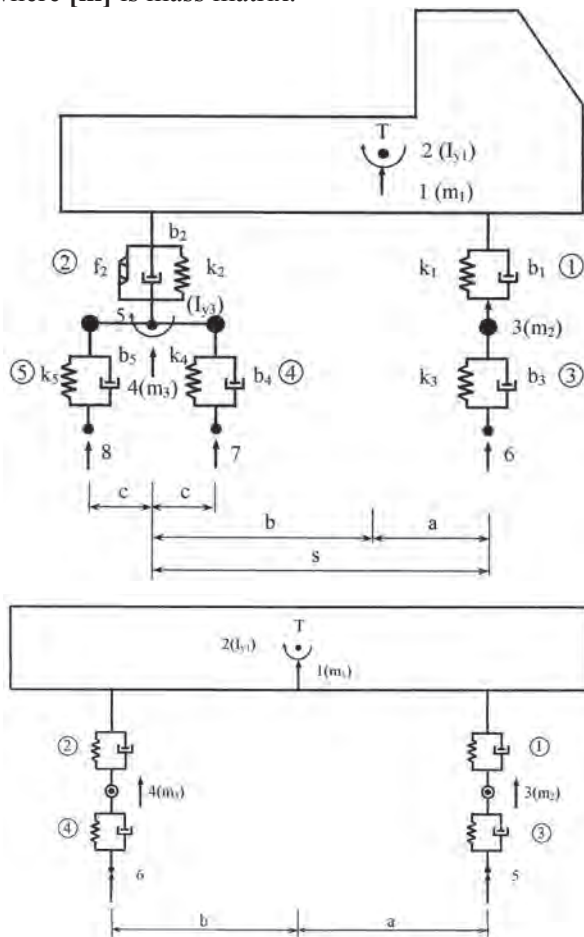
where $[m]$ is mass matrix.

Fig. 1. Plane computing models of a lorry and a bus

3. Computing model of a bridge

For the description of bridge vibration the simplified computing model in the form of simply supported Euler beam excited by moving forces is adopted, Fig. 2.
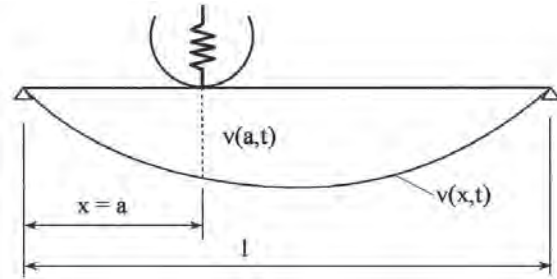

Fig. 2. Computing model of a bridge as a simply supported Euler beam

Equation of motion can be written as

$$E \cdot I \cdot \frac{\partial^4 y(x,t)}{\partial x^4} + \mu \cdot \frac{\partial^2 y(x,t)}{\partial t^2} + $$
$$+ 2 \cdot \mu \cdot \omega_b \cdot \frac{\partial y(x,t)}{\partial t} = p(x,t) \qquad (9)$$

In the next the following identification will be used: $h(x)$ respectively $h(t)$ – function defining the road unevenness

$y(x,t)$ – dynamic deflection curve of the beam axis

$v(x,t)$ – profile of the runway defined by the term (10)

$$v(x,t) = y(x,t) + h(x) \qquad (10)$$

The assumption about the shape of dynamic deflection curve is adopted in the form

$$y(x,t) = f(t) \cdot \psi(x,t) \qquad (11)$$

where $f(t)$ is a coefficient of proportionality dependent on the time t and $\psi(x,t)$ is the static deflection curve induced by static effect of vehicle.

$$\psi(x,t) = \sum_{n=1}^{\infty} \eta_n(t) \cdot \sin \frac{n \cdot \pi \cdot x}{l} , \qquad (12)$$

where

$$\eta_n(t) = \frac{2}{E \cdot I} \cdot \left(\frac{l}{\pi}\right)^4 \cdot \frac{1}{l} \cdot$$
$$\cdot \left(\sum_{j=1}^{m} \varepsilon_j \cdot \frac{G_j}{n^4} \cdot \sin \frac{n \cdot \pi \cdot x_j}{l} \right) \qquad (13)$$

l is span of the beam, G_j is weight j-th vehicle axis. Coefficient $\varepsilon_j = 1$, if the corresponding axis is on the bridge and $\varepsilon_j = 0$, if the corresponding axis is outside the bridge. For the practical use only the 1st member

of infinite series is used for the calculation. Than

$$\psi(x,t) = \eta_1(t) \cdot \sin\frac{\pi \cdot x}{l} \qquad (14)$$

and in the case of plane computing model of vehicle

$$\eta_1(t) = \frac{2}{E \cdot I} \cdot \left(\frac{l}{\pi}\right)^4 \cdot \frac{1}{l} \cdot \left(\sum_{j=1}^{m} \varepsilon_j \cdot G_j \cdot \sin\frac{\pi \cdot x_j}{l}\right) \qquad (15)$$

Expression for $y(x,t)$ than can be written as

$$y(x,t) = f(t) \cdot \psi(x,t) =$$
$$= f(t) \cdot \eta_1(t) \cdot \sin\frac{\pi \cdot x}{l} = q(t) \cdot \sin\frac{\pi \cdot x}{l} \qquad (16)$$

and expression for the profile of the runway is

$$v(x,t) = y(x,t) + h(x) = q(t) \cdot \sin\frac{\pi \cdot x}{l} + h(x) \qquad (17)$$

$q(t)$ in equations (16) a (17) is generalized Lagrange coordinate. Assume that $y(x,t) = q(t) \cdot \sin(\pi \cdot x / l)$, than

$$\frac{\partial^4 y(x,t)}{\partial x^4} = q(t) \cdot \frac{\pi^4}{l^4} \cdot \sin\frac{\pi \cdot x}{l} \qquad (18)$$

$$\frac{\partial^2 y(x,t)}{\partial t^2} = \ddot{q}(t) \cdot \sin\frac{\pi \cdot x}{l} \qquad (19)$$

$$\frac{\partial y(x,t)}{\partial t} = \dot{q}(t) \cdot \sin\frac{\pi \cdot x}{l} \qquad (20)$$

After substitute (18), (19), (20) into equation (9) we obtain

$$E \cdot I \cdot q(t) \cdot \frac{\pi^4}{l^4} \cdot \sin\frac{\pi \cdot x}{l} + \mu \cdot \ddot{q}(t) \cdot$$
$$\cdot \sin\frac{\pi \cdot x}{l} + 2 \cdot \mu \cdot \omega_b \cdot \dot{q}(t) \cdot \sin\frac{\pi \cdot x}{l} = p(x,t) \qquad (21)$$

respectively

$$\left\{\ddot{q}(t) \cdot \mu + \dot{q}(t) \cdot 2 \cdot \mu \cdot \omega_b + q(t) \cdot E \cdot I \cdot \frac{\pi^4}{l^4}\right\} \cdot$$
$$\cdot \sin\frac{\pi \cdot x}{l} = p(x,t) \qquad (22)$$

The moving forces $F_{int,j}$ can be transform by the use of Dirac δ function on the continual load

$$p(x,t) = \sum_j \varepsilon_j \cdot \delta(x - x_j) \cdot F_{int,j}(t). \qquad (23)$$

For the plane computing model we can write

$$p(x,t) = \sum_j \varepsilon_j \cdot \delta(x - x_j) \cdot F_{int,j}(t) =$$
$$= \sum_j \sum_{n=1}^{\infty} p_{n,j}(t) \cdot \sin\frac{n \cdot \pi \cdot x}{l} \qquad , \qquad (24)$$

where

$$p_{n,j}(t) = \frac{2}{l} \int_0^l p_j(x,t) \cdot \sin\frac{n \cdot \pi \cdot x}{l} \cdot dx =$$
$$= \frac{2}{l} \cdot \varepsilon_j \cdot F_{int,j}(t) \cdot \sin\frac{n \cdot \pi \cdot x_j}{l} \qquad (25)$$

Than

$$p(x,t) = \sum_j \sum_{n=1}^{\infty} p_{n,j}(t) \cdot \sin\frac{n \cdot \pi \cdot x}{l} =$$
$$= \sum_j \sum_{n=1}^{\infty} \frac{2}{l} \cdot \varepsilon_j \cdot F_{int,j}(t) \cdot \sin\frac{n \cdot \pi \cdot x_j}{l} \cdot \sin\frac{n \cdot \pi \cdot x}{l} =$$
$$= \sum_j \sum_{n=1}^{\infty} \frac{2}{l} \cdot \sin\frac{n \cdot \pi \cdot x}{l} \cdot \varepsilon_j \cdot F_{int,j}(t) \cdot \sin\frac{n \cdot \pi \cdot x_j}{l} \qquad (26)$$

When we will use only the 1st member of the series than the expression for $p(x,t)$ can be simplified

$$p(x,t) = \frac{2}{l} \cdot \sin\frac{\pi \cdot x}{l} \cdot \sum_j \varepsilon_j \cdot F_{int,j}(t) \cdot \sin\frac{\pi \cdot x_j}{l} \qquad (27)$$

4. Results of numerical calculations

Numerical calculations were realised in the environment of the program system MATLAB. For the purpose of numerical calculations the parameters of the prestressed concrete bridge with the span $l = 29,0$ m were used. Moment of inertia of the cross section $I = 1,60622$ m^4, modulus of elasticity $E = 3,85e10$ N·m^{-2}, intensity of the mass $\mu = 19680$ kg·m^{-1}, circular frequency of damping $\omega_b = 0,1$ rad·s^{-1}. From the aspect of bridge designers the values of dynamic coefficients versus speed of vehicle motion are interested. Therefore in the next the values of dynamic coefficients δ versus speed of vehicle motion in interval of $V = 0 – 120$ km/h are presented, Fig. 3, 4. As the moving vehicles the lorry Tatra T815 and the bus KAROSA with following parameters are applied.

Tatra T815:

$m_1 = 22\ 950$ kg, $m_2 = 910$ kg, $m_3 = 2\ 140$ kg, $I_{y1} = 62\ 298$ kg·m^2, $I_{y3} = 932$ kg·m^2,

$k_1 = 287\ 433$ N/m, $k_2 = 1\ 522\ 512$ N/m, $k_3 = 2\ 550\ 600$ N/m, $k_4 = k_5 = 5\ 022\ 720$ N/m,

$b_1 = 19\ 228$ kg/s, $b_2 = 260\ 197$ kg/s, $b_3 = 2\ 746$ kg/s, $b_4 = b_4 = 5\ 494$ kg/s.

Initial conditions are assumed as:

$r_1(0) = -0,02$ m, $\dot{r}_1(0) = 0,0$

m/s, $r_2(0) = 0,0$ m, $\dot{r}_2(0) = 0,0$ m/s,

$r_3(0) = -0,002$ m, $\dot{r}_3(0) = 0,0$ m/s,

$r_4(0) = -0,003$ m, $\dot{r}_4(0) = 0,0$ m/s,

$r_5(0) = 0,0$ m, $\dot{r}_5(0) = 0,0$ m/s.

The function $\delta(V)$ is not smooth curve. It has many local maxima and spikes. Its character is connected with discontinuities in the function $x_t(V)$ indicating the position of vehicle on the bridge at the moment of arising of maximal dynamical deflection in the mid span of the bridge. The position of spikes in the function $\delta(V)$ corresponds to the position of discontinuities in the function $x_t(V)$, Figs. 3, 4.

Fig. 3. Dynamic coefficients and position of vehicle versus speed of vehicle motion, T815
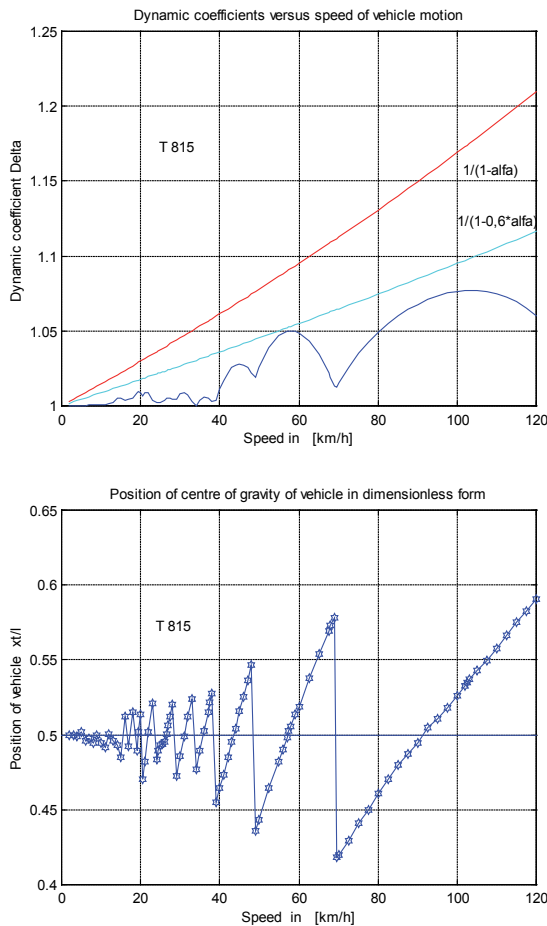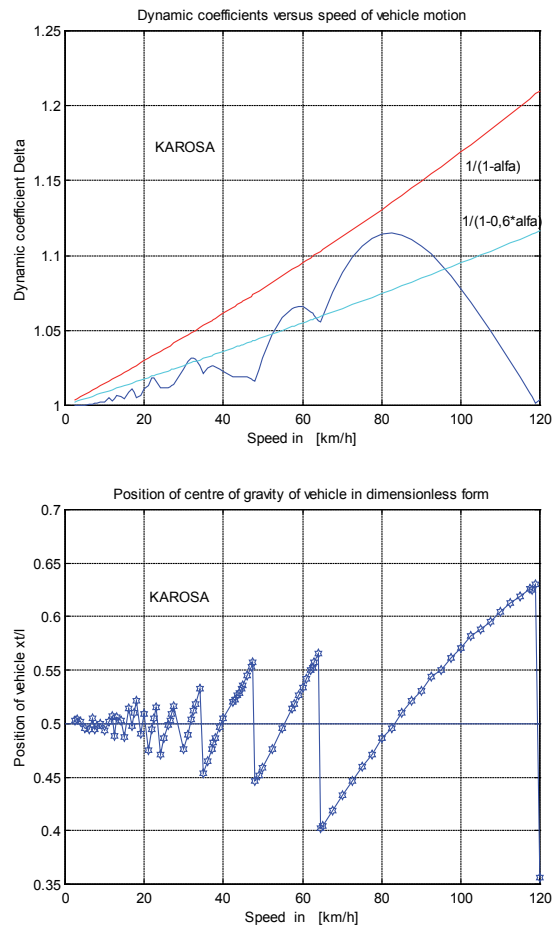

Fig. 4. Dynamic coefficients and position of vehicle versus speed of vehicle motion, KAROSA

KAROSA:

$m = 18\ 150$ kg, $m_1 = 600$ kg, $m_2 = 1\ 250$ kg, $I_y = 330\ 420$ kg·m²,

$k_1 = 850\ 000$ N/m, $k_2 = 1\ 500\ 000$ N/m, $k_3 = 1\ 700\ 000$ N/m, $k_4 = 3\ 400\ 000$ N/m,

$b_1 = 80\ 000$ kg/s, $b_2 = 160\ 000$ kg/s, $b_3 = 4\ 000$ kg/s, $b_4 = 8\ 000$ kg/s.

Initial conditions are assumed as:

$r_1(0) = -0,02$ m, $\dot{r}_1(0) = 0,0$ m/s,

$r_2(0) = 0,0$ m, $\dot{r}_2(0) = 0,0$ m/s,

$r_3(0) = -0,01$ m, $\dot{r}_3(0) = 0,0$ m/s,

$r_4(0) = -0,009$ m, $\dot{r}_4(0) = 0,0$ m/s.

With respect to the character of the curve $\delta(V)$ it would be convenient to approximate the maximal values of dynamic coefficients by some envelope curve, for example in the shape

$$ok = 1 / (1 - \alpha) \tag{28}$$

or in the shape

$$ok = 1 / (1 - 0,6\alpha). \tag{29}$$

The dimensionless coefficient α indicates the influence of the speed of vehicle motion. It is defined as

$$\alpha = T_{(1)} / 2T_P \tag{30}$$

$T_{(1)}$ is the period of bridge vibration in the 1st natural mode and T_P is the transit time of one axle along the bridge. Every type of vehicle has its own suitable envelope curve. But envelope curve (28) covers all cases.

References

[1] Willis, R.: *Appendix, Report of the Commissioners Appointed to Inquire into the Application of Iron to Railway Structures.* Stationary Office, London 1849.

[2] Impact on Highway Bridges. *Final Report of the Special Committee on Highway Bridges, Transactions ASCE*, Vol. 95, 1931, pp. 1089-1117.

[3] Huang, T.: *Vibration of Bridges*. Shock and Vibration Digest, Vol. 8, No. 3, 1976, pp. 61-76.

[4] Frýba, L.: *Dynamika železničních mostů.* ACADEMIA, Praha 1992.

[5] Melcer, J.: *Dynamické výpočty mostov na pozemných komunikáciách*. EDIS, Žilinská univerzita v Žiline, 1997.

structure

JACEK ŚLUSARCZYK

Kielce University of Technology,
Al. Tysiąclecia Państwa Polskiego 7,
25-314 Kielce, Poland,
e-mail: jaceks@tu.kielce.pl

RELATIONSHIP M(κ) ON THE BASIS OF RESEARCH ON BEAMS SUBJECTED TO CHANGING LOADS

Abstract

While calculating reinforced concrete constructions the relationship momentum – curvature M(κ) has significant importance. In exploitation conditions reinforced concrete construction is subjected to increasing loading and unloading. In bent moments, performing even a few cycles of static loading and unloading causes increase in temporary deflection. Building a unified model of relationship M(κ) describing the whole range from the elastic state to the full plasticisation, allowing for variable reversible loads (hysteresis loop) requires further investigations. Degradation of cross section stiffness is the result of damage process and plasticisation. Unified description of processes taking place in reinforced concrete beam cross section can be obtained with the use of elastic work probability, plastic work probability and damage relating cross section stiffness.

Keywords: concrete beams, changing loads

1. Introduction

The relationship moment – curvature $M(\kappa)$ has special meaning for calculating reinforced concrete constructions. It determines distribution of internal force in static non-determinable states and measures of element deflections. The relationships $M(\kappa)$ presented in papers [1-4] allows to calculate reinforced concrete loaded with monotonically increasing instantaneous or long-lasting load.

Theoretical recognition of the relationship $M(\kappa)$ in the process of loading by basic methods can be found in ([5], [6]). Obtained numerically theoretical relationships are strongly determined by the assumption of linear-elastic behaviour of unloaded concrete and steel with the unloading modules equal to the initial values in the process of loading. Applying the simplified material relationships for concrete cross section behaviour neglects specific features of reinforced concrete cross section behaviour in the process of unloading. In the reinforced concrete cross section appear mechanisms related to micro and macro cracks [7], plasticisation and self-stress [8].

In elements subjected to bending, performing even a few cycles of static loading and unloading causes increase in temporary deflection. Building a unified model of $M(\kappa)$ describing the whole range from the elastic state to the full plasticisation allowing for variable reversible loads (hysteresis loop) required relevant investigation.

The purpose of this paper is to present a proposal of constitutive relationship that is valid not only in the process of increasing loads but unloads as well, showing its real characteristics. Extending the relationship $M(\kappa)$ by unloading processes allows for its history. It is required to perform the analyses of bent reinforced concrete rod constructions which undergo the static loading. The occurring plasticisation and damage processes by unloading should be estimated experimentally. The knowledge of $M(\kappa)$ while unloading is indispensable not only for the calculation of the deflection of elements with changing loads, but also for the determination of the force redistribution in the structures statically indeterminable. In the first part of the paper a theoretical analysis of the continual relationship moment-curvature $M(\kappa)$ has been carried out. In the second part, it was possible to determine the values of the unknown model functions on the basis of the results of the experimental investigation.

2. Relationship M(κ) in the process of reproducible loads

2.1. General process description

Any history of cross section loading can be presented as a sequence of curvature quantities (measure) $\{\kappa_i\}$ = $\{\kappa_0 = 0, \kappa_1, \kappa_2, ... \kappa_n\}$ and corresponding moment quantities $\{M_i\}$ determining points of change in load direction. Separated by two subsequent curvature quantities, relationship course $M - \kappa$ will be called a 'branch' of the loading process. To simplify the notation, for every branch we will accept local coordinate system of coefficients κ'_i, M'_i oriented according to curvature direction change (see Fig. 1). Relationships occur between the global and local coordinate systems:

$$\kappa = \kappa_{i-1} \pm \kappa'_i \Rightarrow M = M_{i-1} \pm M'_i$$

The plus occurs for loading branches and minus for unloading ones.

2.2. Cross section model

Degradation of cross section stiffness is the result of damage and plasticisation processes. Theoretical basis for such a model has been described by Goszczyński S. [9]. Unified description of processes taking place in reinforced concrete beam cross section can be obtained with the use of elastic work probability, plastic work probability and damage relating to cross section stiffness. During loading, the degree (probability) of cross section plasticising and damage rises, whereas, for the sake of simplification, it can be assumed that these processes are independent from each other. During unloading, stresses of opposing signs additionally degrading stiffness appear in the part of the plasticised cross section zone. In this case, too, independence of the plasticising and damage processes can be postulated but the probabilities determining advancement of these processes are conditional probabilities dependants on the degree of the cross section plasticising during loading. Under the assumptions, function $M'_i(\kappa'_i)$ for 'i' branch can be described by the formula

$$M'_i = (B_o \kappa'_i E_i + P_i M_{pi}) N_{pi} N_{wi} \qquad (2.1)$$

where:
B_o – cross section stiffness in the phase Ia,
i – number of load interval,
κ'_i – absolute curvature increase quantity,
E_i, P_i – probability functions of elastic and plastic work,
M_{pi} – function of moment quantity carried by plasticised cross section,

$N_{pi} = N_{p1} - R_{pi}$ – probability functions of non-damaging by loading,
$N_{wi} = N_{w1} - R_{wi}$ – probability functions of non-damaging the cross section by loading,
R_{pi} – probability functions of damaging by loading,
R_{wi} – probability functions of damaging the cross section by loading.

Since all functions marked with bold italics depend on curvature increase, absolute variables have been omitted in notations.

Two definitions of stiffness are used: secant stiffness marked as B and called shortly "stiffness" with its final value B_i and "instantaneous stiffness" marked as $B(\kappa')$, and its initial value as B_{oi}.

Undamaged part of the cross section works partly elastically and in the rest part plastically, thus at every moment we have

$$E_i + P_i = 1. \qquad (2.2)$$

After changing load direction, initially, the whole of undamaged cross section works elastically – the process of plasticising is fully and immediately reciprocal. It causes instantaneous stiffness jump. Initial stiffness of subsequent unload branches is bigger than final stiffness of the previous load branch. During the next loading, the previous state of plasticising the cross section is restored at the moment of exceeding the maximum curvature, causing visible decrease of instantaneous stiffness.

Increase of the stiffness observed during the investigation in the initial intervals of the branch, especially with big load changes, can be explained by pseudo-regeneration of cross section. Since damage relates primarily to concrete being stretched, after changing the direction of load micro cracks and even cracks close. The concrete in these areas starts conveying compression. Thus 'empowering' the cross section will be obtained, assuming reciprocity of damage processes. In contrast to plasticising processes, regeneration is not complete (it occurs with probability $p = 0$). Taking into consideration regeneration it leads to characteristic, 'S' shape of the branch. Such phenomenon has not been observed yet in the results.

During loading, the initial function quantity N_{wi} equals final quantity from the proceeding unloading branch. If there is no cross section regeneration, the function remains constant for the whole branch, otherwise, it is an ascending function. Function N_{pi} has analogical features while unloading.

The process of loading proceeds in time causing rheological effects: creeping and relaxation decreasing stiffness. Changeability of load, even low cycling, increases these effects. During short-lasting investigation, "early rheologism" with big, but quickly descending velocity of deformation growth plays an important role. This means decrease of stress. It leads to, after a short period of time or after some teen cycles, stability of the branch. In the presented model describing the process of instantaneous loads, time-independent influence of early rheological phenomena is treated as damage.

In case of monotonic probability function, certain branches are also monotonic functions and theoretical relationship $M - \kappa$ presented in Fig. 2. It indicates representation possibility of real proceeding of this relationship.

2.3. The first branch – loading

If we neglect the results of internal stress caused by concrete ageing, the process of constantly growing load is characterised by function constancy $N_{w1} = N_{w0} = 1$ and initial function values: $N_{p1}(0) = N_{p0} = 1$, $P_1(0) = 0$ **and** $E_1(0) = E_0 = 1$. Yet the differences observed in the research (e.g. [10], [11]) of initial beam stiffness indicate that these phenomena have significant influence and therefore should be taken into account. In the form of the presented model it means that initial values of the functions discussed do not follow previously described relationships and there is $N_{p0} < 1$, $N_{w0} < 1$. It would be possible to observe the occurrence of the initial plasticising in case of asymmetric reinforcement as the difference in initial stiffness for bending moments of opposing signs. So far no data is available which would confirm the occurrence of this phenomenon.

Plasticising process intensity $f_{P'}$ according to postulated function characteristics must be a constant function. With cross section deformation κ we will obtain plasticising probability

$$P_1 = P_0 + \int_0^{\kappa} f_{P1}(u) \, du = P_0 + \Delta P_1 \approx \Delta P_1, \quad (2.3)$$

and quantity of moment conveyed by plasticised cross section zone

$$P_1 M_{p1} = \int_0^{\kappa} u \, B_o f_{P1}(u) \, du = P_1 \varpi_1 B_o \kappa, \quad (2.4)$$

where: $0 < \varpi < 1$ – determines the ratio of moment conveyed by plasticised cross section and elastically working cross section.

f_{P1} – intensity of plasicising process with deformation κ. applying the introduced notation, we will obtain the quantity of the moment equal

$$M = B_o \, \kappa \, [1 - P_1 (1 - \varpi_1)] \, (N_{p0} - \Delta R_{p1}) \, Nw_1, \quad (2.5)$$

where ΔR_{p1} – increase of damage During loading.

Characteristics of cross section work in the initial stage of loading ($\kappa \to 0$) will be obtained from the equation Eq. (2.5). The concrete which is properly cared for has little contraction and in most cases with a small error the following equation can be accepted $N_{w1} = N_{w0} = 1$. After omitting small higher dimensions the equation has the form

$$M = N_{p0} \, B_o \, \kappa = B_{o1} \, \kappa \, . \quad (2.6)$$

Initial stiffness B_{o1} equals tangent of tangent slope at the point $\kappa = 0$ and can be determined directly from the experiment results. This enables calculating initial non-damage of cross section

$$N_{p1}(0) = B_{o1} / B_o = N_{p0}. \quad (2.7)$$

Instantaneous stiffness of the first branch can be obtained by differentiation of the equation Eq. (2.1)

$$B(\hat{e}) = \left(B_o \, E + B_o \, \hat{e} \left| \frac{\partial E}{\partial \hat{e}} \right| + \left| \frac{\partial P}{\partial \hat{e}} \right| M_p + \left| \frac{\partial M_p}{\partial \hat{e}} \right| P \right) N_p \, N_w +$$

$$+ \left(B_o \, \hat{e} \, E + P \, M_p \right) \left(\left| \frac{\partial N_p}{\partial \hat{e}} \right| N_w + \left| \frac{\partial N_w}{\partial \hat{e}} \right| N_p \right) \quad (2.8)$$

It is impossible to determine functions in the equation Eq. (2.1) or Eq. (2.5), on the basis of the empirical function of the first branch.

2.4. The second branch – unloading

Equation of the moments for this branch has the form

$$M'_2 = B_o \, \kappa'_2 \, [1 - P_2 (1 - \varpi_2)] \, N_{p2} \, (N_{w1} - \Delta R_{w2}), \quad (2.9)$$

where: $N_{p2} = N_{p1}$ – probability of non-damage by loading at the moment of unloading,
P_2 – plasticising probability during unloading,
ΔR_{w2} – increase of damage probability during unloading,
ϖ_2 – determines the ratio between the moment conveyed by the cross section plasticised by unloading and the cross section working elastically.

Next we will use the equality of certain initial probability of non-damage, constant for the given branch and final for the proceeding branch.

Initial stiffness for this branch determined from the equation Eq. (2.9), equals

$$B_{o2} = B_o\, N_{p2}\, N_{w1} \qquad (2.10)$$

which enables to calculate the value of non-damage function at this point of the process on the basis of measurement results

$$N_{p2} = N_p(\kappa_1) = B_{o2}\,/\,(B_o\, N_{w1})$$

$$\Delta R_{p1} = 1 - N_{p2} \qquad (2.11)$$

Stretching stress has the biggest influence on stiffness degradation, including during unloading. Since the stretched concrete presents features of a fragile body, the probability of plasticising effects will be small. This means that at least at the first approximation it can be assumed as zero. It allows to simplify the equation Eq. (2.9) as

$$M'_2 = B_o\, \kappa'_2\, N_{p2}\, (N_{w1} - \Delta R_{w2}) \qquad (2.12)$$

describing non-linear, elastic - fragile cross section model. With increasing unload, the probability of damage and stiffness decrease. Its final quantity can be written as

$$B_2 = B_o\, N_{p2}\, (N_{w1} - \Delta R_{w2}) = B_o\, N_{p2}\, N_{w2} \qquad (2.13)$$

Comparing to the final stiffness of the first branch it is bigger since damage probability ΔR_{w2} is the fraction of plasticity probability P_1.

Knowing the initial stiffness and the coefficient of branch ending enables us to calculate the increase of damage ΔR_{w2}:

$$M'_2 = B_o\, \kappa'_2\, N_{p2}\, N_{w2} \Rightarrow N_{w2} =$$

$$= \frac{M'_2}{B_o\, \hat{e}'_2\, N_{p2}} \Rightarrow \Delta R_{w2} = N_{w2} - N_{w1} \qquad (2.14)$$

2.5. The third branch (loading) – deformation hysteresis loop

The subsequent loading, with deformation not exceeding κ_1, gives linear function

$$M'_3 = B_2\, \kappa'_3 = B_{o3}\, \kappa'_3 \qquad (2.15)$$

because subsequent loading does not cause additional damage of the cross section. Also following unloading and loading in the range $<\kappa_1, \kappa_2>$ do not change stiffness; we have a stable loop (unloading – loading) of deformation hysteresis. In the case of fragile material, the loop is reduced to the interval of a straight line.

In reality, obtaining the curvature κ_1 is caused by a smaller moment than M_1 since the influence of rheological phenomena appears. The equation of the third branch, closing the first loop, allowing for rheological effects, assuming $N_{w3} = N_{w2}$, can be presented as follows

$$M'_3 = B_o\, \kappa'_3\, (N_{p2} - \Delta R_{p3})\, N_{w3} \qquad (2.16)$$

where initial stiffness equals zero:

$$B_{o3} = B_o\, N_{p2}\, N_{w3} \qquad (2.17)$$

Increase of damage for $\kappa'_3 = \kappa'_2$ can be calculated analogically as for the second branch:

$$M'_3 = B_o\, \kappa'_3\, N_{p3}\, N_{w3} \Rightarrow N_{p3}$$

$$= \frac{M_3}{B_o\, \hat{e}'_3\, N_{w3}} \Rightarrow \Delta R_{p3} = N_{p2} - N_{p3} \qquad (2.18)$$

To determine the quantity of damage for this branch there can be used difference between moments:

$$\Delta M'_{1,3} = M_1 - M_3 = B_o\, (\kappa'_1 - \kappa'_2)\, \Delta R_{p3}\, N_{w3} \qquad (2.19)$$

While analysing deformation hysteresis loop, it is more convenient to use variables κ'_p for the increasing load and κ'_w for the decreasing one. Loop equations can be generalised for the subsequent m = 1, 2, …, n cycle deformation loops in this interval:

– for unloading branches

$$M'_i = B_o\, \kappa'_w\, N_{p i}\, (N_{w i-1} - \Delta R_{w i}) \qquad (2.20)$$

– for loading branches

$$M'_{i+1} = B_o\, \kappa'_p\, (N_{p i} - \Delta R_{p i+1})\, N_{w i+1} \qquad (2.21)$$

where: i = 2 m.

Initial stiffness of these branches, having allowed for the final of the relevant process at the moment of load direction change, equal respectively:

$$B_{o i} = B_o\, N_{p i-1}\, N_{w i-1} = B_o\, N_{p i}\, N_{w i-1}$$

$$B_{o i+1} = B_o\, N_{p i}\, N_{w i} = B_o\, N_{p i}\, N_{w i+1} \qquad (2.22)$$

The stiffness changes reflect accumulating damages and creeping. They occure as a result of earlier loading. They result from characteristics of loop slope decreasing with the increase of the cycle number.

Increase of the moment for the lower deformation limit (even branch number) in the following cycle ($\Delta\kappa = \kappa_1 - \kappa_2$) amounts to

$$\Delta M'_{i,i-2} = M_i - M_{i-2} = B_o\, \Delta\kappa\, (N_{p i-1}\, N_{w i-1} - N_{p i-1}\, N_{w i})$$

$$= - B_o\, \Delta\kappa\, N_{p i}\, \Delta R_{w i,}$$

and for the upper one

$$\Delta M'_{i+1,i-1} = - B_o\, \Delta\kappa\, \Delta R_{p i+1}\, N_{w i+1} \qquad (2.23)$$

This allows to calculate the range of moment changes after stabilising the deformation hysteresis loop (Fig. 3):

$$M_{min} = M_1 - B_o\, \Delta\kappa\, N_{p2}\, N_{w1} + B_o\, \Delta\kappa \sum_1^m N_{p\,2m}\, \Delta R_{w\,2m}$$

$$(2.24)$$

$$M_{max} = M_1 - B_o \, \Delta\kappa \sum_1^m \Delta R_{p\,2m+1} \, N_{w\,2m} \qquad (2.25)$$

Considering small increases of deformation, equations Eq. (2.24), (2.25) can be simplified as:

$$M_{min} \approx M_1 - B_o \, \Delta\kappa \, N_{p2} \, N_{w1} +$$

$$+ B_o \, \Delta\kappa \, (N_{p2} - \sum_1^m \Delta R_{p\,2m+1}) \sum_1^m \Delta R_{w\,2m} =$$

$$= M_1 - B_o \, \Delta\kappa \, N_{p\,2} \, N_{w\,1} + B_o \, \Delta\kappa \, [N_{p\,2} - \boldsymbol{R_p}(\Delta\kappa)] \, \boldsymbol{R_w}(\Delta\kappa),$$

$$M_{max} \approx M_1 - B_o \, \Delta\kappa \, (N_{w1} - \sum_1^m \Delta R_{w\,2m}) =$$

$$= M_1 - B_o \, \Delta\kappa \, [N_{w1} - \boldsymbol{R_w}(\Delta\kappa)] \qquad (2.26)$$

enabling determination of damage quantity on the basis of measurement.

2.6. The third and the subsequent branches – moment hysteresis loop

Increasing load in the third branch until $M_3 = M_1$ (Fig. 4) causes simultaneously an increase in the curvature until the quantity κ_3. As the consequence we observe not only an increase of damage probability but also an increase of plasticising. The subsequent unloading, as a result of increase in the plasticising degree, increases damage caused by internal stress, as well. There are added rheological effects, too. The undergoing changes in the subsequent cycles $\{i = 2, 4, \ldots, 2n\}$ can be noted as:

$$\begin{aligned}\Delta P_{i+1} &= \boldsymbol{P}(\kappa_{i+1}) - \boldsymbol{P}(\kappa_{i-1}), \\ \Delta R_{p\,i+1} &= \boldsymbol{R_p}(\kappa_{i+1}) - \boldsymbol{R_p}(\kappa_{i-1}), \\ \Delta R_{w\,i} &= \boldsymbol{R_w}(\kappa_i) - \boldsymbol{R_w}(\kappa_{i-2}),\end{aligned} \qquad (2.27)$$

where there have been presented together: damage increase, curvature increase and rheological effects.

If, in the process of cycle loading, the curvature sequence $\{\kappa_{2m+1}\}$ has a finite limit $\kappa_{max} = \kappa_{2n+1}$, then the hysteresis loop is stable in the deformation interval $<\kappa_{min} = \lim\{\kappa_{2n}\}, \kappa_{max}>$. Respective probabilities determining the state of the cross section amount to:

$$\boldsymbol{P_m} = \boldsymbol{P_1} + \sum_{j=1}^n \Delta P_{2j+1} = \boldsymbol{P}(\kappa_{2m+1}) = \boldsymbol{P}(\kappa_{max}),$$

$$R_{p\,m} = R_{p\,1} + \sum_{j=1}^n \Delta R_{p\,2j+1} = \boldsymbol{R_p}(\kappa_{max}), \qquad (2.28)$$

$$R_{w\,m-1} = \sum_{j=1}^n \Delta R_{w\,2j} = \boldsymbol{R_w}(\kappa_{max} - \kappa_{min}),$$

$$N_{p\,m} = 1 - R_{p\,m} = \boldsymbol{N_p}(\kappa_{max}),$$

$$N_{w\,m} = 1 - R_{w\,m} = \boldsymbol{N_w}(\kappa_{max} - \kappa_{min}),$$

and they are the same as in the deformation hysteresis loop $<\kappa_{min}, \kappa_{max}>$.

3. Determining model functions N_p, N_w, E, P, M_p

The relationships between the instantaneous and section stiffness with cycle loads described in point 2 allow to determine damage increase ΔR_p and ΔR_w. As a result, values N_p, N_w model damage functions at the points of changing load direction become known. At the point of initiating the first level of unload cycles, with known $N_{p\,1}$, $N_{w\,1}$ we have the equations Eq. (2.1) and Eq. (2.2). Calculating the values E_1, P_1, $M_{p\,1}$ is still impossible. Similarly, it is impossible at the initial points of the higher unload levels.

The missing equation is the result of instantaneous stiffness quantity at the point of load direction change. At the point of initiating cycle loads for any 'k' level of moment hysteresis loop we have:

$$\left|\frac{\partial \boldsymbol{M}}{\partial \hat{e}}\right|_{\hat{e}_k} = \left(B_0 E_k + B_0 \hat{e}_k \left|\frac{\partial \boldsymbol{E}}{\partial \hat{e}}\right|_{\hat{e}_k} + \left|\frac{\partial \boldsymbol{P}}{\partial \hat{e}}\right|_{\hat{e}_k} M_{p\,k} + \left|\frac{\partial \boldsymbol{M_p}}{\partial \hat{e}}\right|_{\hat{e}_k} P_k\right) N_{p\,k} \, N_{w\,k-1} +$$

$$+ \left(B_0 \hat{e}_k E_k + P_k M_{p\,k}\right)\left(\left|\frac{\partial \boldsymbol{N_p}}{\partial \hat{e}}\right|_{\hat{e}_k} N_{w\,k-1} + \left|\frac{\partial \boldsymbol{N_w}}{\partial \hat{e}}\right|_{\hat{e}_k} N_{p\,k}\right) \qquad (3.1)$$

Little section of empirical relationship $\boldsymbol{M}(\kappa)$ just before the first point of initiating the loop is approximated with a parabola

$$\boldsymbol{M}(\kappa) = a \, \kappa^2 + b \, \kappa + c \qquad (3.2)$$

for which the coefficients a, b, c are determined by the method of the least quares.

As a result, the value of the left side of the equation (3.1) becomes known.

At this point, considering the equations Eq. (2.1), (2.2) and (3.1) we have both unknown E_k, P_k, $M_{p\,k}$ and quantities of model function derivatives $\boldsymbol{E}$, $\boldsymbol{P}$, $\boldsymbol{M_p}$ as well. For initial points of subsequent load levels derivative values $\left|\frac{\partial \boldsymbol{E}}{\partial \hat{e}}\right|_{\hat{e}_k}$ can be determined on the

basis of parabola lead through values E_{k-1}, E_k, E_{k+1}.

The same method is used for derivatives $\left|\frac{\partial \boldsymbol{P}}{\partial \hat{e}}\right|_{\hat{e}_k}$, $\left|\frac{\partial \boldsymbol{M_p}}{\partial \hat{e}}\right|_{\hat{e}_k}$. Equations (2.1), (2.2) and (3.1) noted for the initial point of 'k' unload level contains nine unknowns E_{k-1}, E_k, E_{k+1}, P_{k-1}, P_k, P_{k+1}, $M_{p\,k-1}$, $M_{p\,k}$,

$M_{p\ k+1}$. Equations (2.1), (2.2) and (3.1) for all initial points of loading levels form a system of the same number of equations as the unknowns. Due to non-linearity of these equations model function values $E_1, \ldots, E_{k-1}, E_k, E_{k-1}, \ldots, E_n, P_1, \ldots, P_{k-1}, P_k, P_{k-1}, \ldots, P_n, M_{p1}, \ldots, M_{p\ k-1}, M_{p\ k}, M_{p\ k-1}, \ldots, M_n$, for points initiating cycles they are determined numerically with the use of Newton method [12].

4. Experimental research of three span reinforced concrete beams.

It is characteristic of the publicised research results of continuous reinforced concrete beams [13-15] that the research programs are limited to the issues of interest for the different researchers.

Experimental discovery of the cross section and an element work with temporary load (without dynamic effects) considering the unloads have been carried out on three span reinforced concrete beams. It was necessary to carry out the experiment in Independent School of Reinforcement Construction and Industrial Building of Technical University of Kielce due to lack of research results allowing to determine model function values of relationship M(κ).

The static scheme of three span continuous beam has been accepted (Fig. 5), with rectangular cross section 140 x 250 mm, and the length of peripheric spans 1750 mm and midspan 2750 mm. The beams were made of concrete with average resistance to compression about 22 MPa. Percentage of reinforcement with bars # 12 from steel 34 GS amounted to 1.07%.

Two beams have been tested '1' and '2'. Two focused forces applied in the midspan formed the load. The program of static load (controlling of focused force P) were done according to scheme $P = 0 \rightarrow P_1 \leftrightarrow 0 \rightarrow P_2 \leftrightarrow 0 \rightarrow P_3 \ldots$, where $P_i > P_{i-1}$, P_U – damaging force. The number of loading and unloading cycles from the given force level P was dependant on measurable hysteresis loop stability force - deflection.

During measurement program for the tested elements were registered:

- the quantity of the applied load P and all the reactions on the supports: A, B, C, D (see Fig. 6)
- deflection in the determined points of the beams (see Fig. 6)
- deformation of upper and lower fibres on both sides of the beam (see Fig. 6)
- location, height and opening of cracks.

Testing of continuous beams was carried out on a measuring stand.

For the measurements the following devices were used:

- box dynamometers (range 25 – 160 kN) for measuring applied load and bearing reaction; estimated on the basis of calibration of max measured force error for the different dynamometers from 0.19 – 0.44 kN,
- induction sensors by PELTRON (range 50 – 100 mm) for measuring deflection; accuracy 1.25 x 10^{-5} m,
- extensometer type MAYES (range 200 mm) for measuring deformation; accuracy 0.8 x 10^{-5}
- Brinell microscope (enlargement 24 times) for measuring crack opening.

The quantity of the applied load, bearing reaction and deflection, were registered with thirty two channel analogue – digital converters mounted into an IBM PC. This allowed to gather a large number of measuring points. The converter with jump load increase P for the assumed level, sampled automatically five times with the same load kept, every 20 seconds for 5 minutes.

5. Empirical hysteresis loops and their analysis.

For the interval of sheer bending in the span $M(\kappa)$ has been calculated on the basis of the measured deformations and deflections. There the constant intensity of longitudinal reinforcement exists simultaneously. The calculated relationships $M(\kappa)$ differed maximally by ~12%. The confirmed reliability of the results computed from automatic measurement of deflection allowed to base the analysis exclusively on them.

The experimental curvature was calculated based on the formula:

$$\kappa = \mathbf{8} \, \Delta f / \, l^2 \tag{5.1}$$

where: Δf – the increase in the deflection in the middle of the segment l in relationship to its ends l – the length of the segment of sheer bending. Chosen as an example two series of moment loops M(κ) for one of the beams have been shown in (Fig. 7). They are both with the ranges respectively ~26 – 0 kNm and ~29 – 0 kNm. For each series there are from several to several teens unloading and loading branches lying close to each other. Due to the measurement carried out only in a few points of the branch, linking results are presented as broken line. Observed subsequent branch overlapping, overlaying, crossing may be explained both by the character of the phenomenon and the measuring accuracy.

The obtained empirical points with coefficients (M, κ) in the Cartesian system are loaded with errors ΔM and Δκ, resulting from the accuracy of measured bearing reactions, applied load and deflection

measurement. On the basis of measuring equipment calibration [15] maximal value of span moment error $\Delta M_g = 1.23$ kNm and curvature error $\Delta \kappa_g = 0.0002$ 1/m have been estimated.

In order to determine the shape of 'm' loop from the sequence, the following analysis has been carried out. For any empirical point 'L' with coefficients (κ_L, M_L) lying on the load or unload curve (Fig. 8) vertical distances -ΔM_L and horizontal ones $\Delta \kappa_L$ from the straight line run through the upper and lower vertex of the loop have been calculated. It arises from the statistic comparison of the sets of the vertical $\{\Delta M_L\}$ and horizontal $\{\Delta \kappa_L\}$ distances to maximal measuring errors of the moment $\Delta M_g = 1.23$ kNm and curvature $\Delta \kappa_g$ that the loop $M(\kappa)$ can be linearised in the loading and unloading process.

The sequence of hysteresis loop has been limited by the contour of a quadrangle as in Fig. 9.

Unloads and repeated loads cause additional damage process which is proved by positive sums of temporary and permanent curvature increase. Having formed the sequence of hysteresis loops from any point 'k' on the original curve $M^0(\kappa)$, we do not get to the lengthening of the curve (Fig. 9).

6. Probability values E, P, N_p, N_w and moment quantity M_p in the initial unload points of 'κ' load level with estimation of errors ΔE, ΔP, ΔN_p, ΔN_w, ΔM_p.

The determined relationship $M(\kappa)$ for the middle beam interval of 1000 mm length served for calculating values of model functions E, P, N_p, N_w, M_p. Relationship $M(\kappa)$ is loaded with error of bending moment ΔM_g resulting from accuracy of bearing reaction measurement [16]. Curvature error $\Delta \kappa_g$ has been omitted considering it a small one in comparison with maximal calculated curvature.

If the calculated quantity depends on many supporting quantities, there is a very small probability of occurrence of an event in which errors of all supporting quantities will take extreme values and unfavourable set of signs. The best results can be obtained if we treat the measuring results together with its error as a random variable. In this case, in order to estimate its error, we can use radical form variation called an absolute probable average error [17].

If for the random variable

$$Y = f (X_1, X_1, ..., X_n) \qquad (6.1)$$

non-linearity of the function f has little importance and coefficients of variable changing X_i are not too big, then approximation of the variable variation Y in the most general case is as follows

$$Var[Y] \approx \sum_{i=1}^{n} \sum_{j=1}^{n} \frac{\partial f}{\partial X_i} \frac{\partial f}{\partial X_j} Cov[X_i, X_j] \qquad (6.2)$$

where: $Cov[X_i, X_j]$ means covariantion of variables X_i, X_j.

Due to independence of variables X_i covariantion are zero and then

$$Var[Y] \approx \sum_{i=1}^{n} \left(\frac{\partial f}{\partial X_i} \right)^2 Var[X_i]. \qquad (6.3)$$

In the analysis, it has been assumed that function values E, P, N_p, N_w, M_p are loaded with errors because of bending moment error ΔM_{gmax}. It arises from the analysis of bearing reaction [16] that for any point of the empirical relationship $M(\kappa)$ the calculated ordinate is the expected value of the bending moment. It follows the normal distribution with standard deviation equalling one third ΔM_{gmax}. Estimating the errors ΔE, ΔP, ΔN_p, ΔN_w, ΔM_p we calculate the radicals from variation which is standard deviation.

Obtaining directly the analytical formulas of errors ΔE, ΔP, ΔN_p, ΔN_w, ΔM_p with the use of (6.2) or (6.3) is impossible. The most accurate solution is to make use of the probabilistic nature of errors ΔE, ΔP, ΔN_p, ΔN_w, ΔM_p stemming from the bending moment error ΔM_{gmax}. For this purpose, its necessary to sample the value of the moment random variable for subsequent measuring points of the relationship $M(\kappa)$ with the application of elemental simulation. In an artificial manner for the relevant measuring points (κ, M) the values of random variable M have been generated. Variability according to normal distribution with expected value equal to empirical bending moment value in the given point and standard deviation of one third value of ΔM_{gmax} have been assumed. The normal distribution was generated with Monte Carlo simulation method [18].

While estimating error values ΔE, ΔP, ΔN_p, ΔN_w, ΔM_p thirty simulations have been carried out. They yield a set of thirty curvatures $M(\kappa)$ for every beam. Numerically determined thirty-element sets with Newton method E, P, N_p, N_w, M_p were used for calculating average values and standard deviations. The determined maximal in the observed range of loads relative error values δE, δN_p, δN_w, δM_p equal respectively 13.1, 6.4, 4.3, 12.8 [%].

The course of the determined model function values E, P, N_p, N_w, M_p in the function of effort M/M_u (M_u - empirical damage moment) is presented graphically in Fig. 10. M_u is known as a result of the created plastic coupling on the section of sheer bending for both tested beams.

The experimental research presented in this paper with analysis of the obtained results allows us to state the following:

- in the range of loads up to ~0.9 of damage moment the influence of unloads on reinforced concrete beams is small. There is only observed damage increase of cross section stiffness of ~15-18%,
- the process of damage during loading is significant as for effort ~0.9 probability of cross section damage amounts to 59-66%,
- cross section plasticising probability in the researched range increases on average from 40 to 85%,
- in the load range up to ~0.65 M_u a small increase of probability elastic work maximally up to ~5% is observed. This indicates bigger concentration of damage in the plasticised parts of cross section,
- for practical uses hysteresis loop in the changing load process can be linearised; the slope angle of the straight line depends only on the product of values of non-damage probability $N_{p\,k}\,N_{w\,k}$.

The obtained values of the model function reflect quantitative influence of damaging processes and plasticisation on cross section stiffness degradation with the accepted mathematical model (2.1). Physical interpretation of the model functions stems from treating the cross section as a set of elementary sectors behaving elastically, plastically and in a short way for any yield point and deformation point being random variables.

7. Summary

The relationship M(κ) valid not only for the process of increasing load but also unloading is suggested in this paper. It is continual, non-linear limited to five model functions E, P, N_p, N_w, M_p reflecting its real character. Physical interpretation of model functions stems from the following assumptions:

- the cross section is treated as a set of material points with random mechanical features,
- elementary sectors behave in an elastic, plastic and in a short way, with yield point and deformation point being random variables,
- the features on the level of the cross section are represented by respective values of the five functions or their proper combinations in the accepted mathematical model.

The model generalises theoretical descriptions of relationships M(κ) in the processes of loading and unloading. The model functions reflect mechanisms related to micro and macro cracking, plasticising and self-stress. The simplicity and clarity is the advantage of so formed relationship. Thus, its not necessary to analyse the relationships between deformation, normal stress or adhesion stress between two neighbouring cracks.

The values of the unknown model functions have been determined on the basis of the small database of experiment results of M(κ) allowing for low-cycle loading. This limits the validity of the model to the specific cross section shape with given percentage content of reinforced steel both for stretching and compressing, its kind and concrete characteristics.

The small number of the tested beams together with the existing estimated errors ΔE, ΔP, ΔNp, ΔN_w, ΔM_p about ~13% call for caution in the quantitative evaluation of the individual processes. For practical uses hysteresis loop in the changing load process can be linearised. The slope angle of the straight line depends only on the product of values of non-damage probability $N_{p\,k}\,N_{w\,k}$.

For a better quantitative evaluation of the damage and cross section plasticisation processes it is required to carry out broader experimental research.

References

[1] Czkwianianc A., Kamińska M.: *Method of non-linear analysis of reinforced iron rod's elements.* Engineering Studies nr 36, Warsaw 1993.

[2] Pawlikowski J.: *Relations formed during analysis in bar reinforced constructions.* ITB, Warsaw 1992.

[3] Wranik J.: *Calculation of rigidity in reinforced constructions based on non-linear elasticity model.* Scientific Notebook from Zielona Góra University. Zielona Góra 2003.

[4] Knauf M. et. al.: *Fundamentals for design of the reinforced and stressed consctructions according to Eurocode 2.* Concrete Section of the Polish Academy of Sciences (KILiW PAN). DWE, Wrocław 2006.

[5] Bąk G., Szczeniak Z.: *Integral physic's principle for bent reinforced cross-section. Part I – Loading process, Part II – Unloading process.* Bulletin of the Military Technical Academy (WAT) nr 10 (350), 1981.

[6] Bąk G., Szczeniak Z.: *Generalized physical relations holding for eccentricly compressed cross-sections.* AIL, t. XXXVII, z. 3-4, 1991.

[7] Hoła J.: *Initial and critical compressive stress and rupture in compressed concrete.* Scientific Papers of IB PW, Wrocław 2000.

[8] Ubysz A: *Plastic strain and self-stress in bar reinforced concrete constructions.* Scientific Papers of IB PW, Wrocław 1999.

[9] Goszczyński S.: *Theory of continuous rigidity changes upon stochastic model of the reinforced concrete.* Scientific Papers of Technical University Kielce, Civil Engineering, 23/1986.

[10] Goszczyński S.: *Hypothesis of exponential rigidity changes in bend reinforced concrete beams*, Scientific Conference Notebook (WBL PŁ), Łódź 1971.

[11] Goszczyński S., Mucha J.: *Problem of initial and recurrent rigidity in bend beams from reinforced concrete elements in view of experimental investigations*. Scientific Papers of Technical University Kielce, Civil Engineering, 9/1980.

[12] Zboś D.: *Numerical methods*. Wyd. PK, Kraków 1991.

[13] Kordina K.: *Load-carrying ability and deformation in reinforced beams under bend and simultaneous constrainment as result of support dispalacement*, DafST H. 336. Berlin 1982.

[14] Kuczyński W., Tkaczyk S.: *Study of continuous reinforced concrete beams*, AIL XXVII, nr 4, s. 559-583/1981.

[15] Goszczyński S., Ślusarczyk J: *Approximation of secant rigidity considering calculation error based on applied research*. XLII Scientific Conference of the Polish Academy of Sciences, (KILIW PAN I KN PZITB), 75-82, Krynica 1996.

[16] Ślusarczyk J.: *Measurement reaction of the three bay reinforced beam considering the error calculus*. Polish Academy of Science in Wroclaw Board of Building Engineering and Mechanics - Concrete constructions - Theory and experimental studies, pp. 50 – 62, Wrocław 1999.

[17] Jaworski J.: *Matematical Fundamentals in metrology*. WNT, Warsaw 1979.

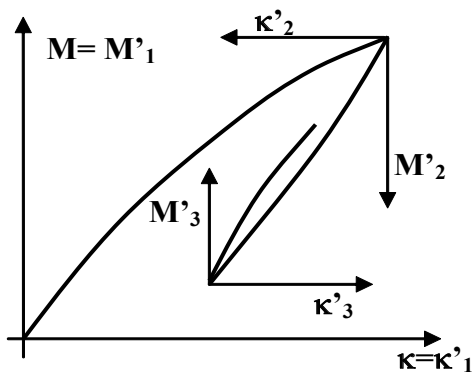[18] Benjamin J.R., Kornel C.A.: *Probability, statistics and decision theory for engineers*. WNT, Warsaw 1977.
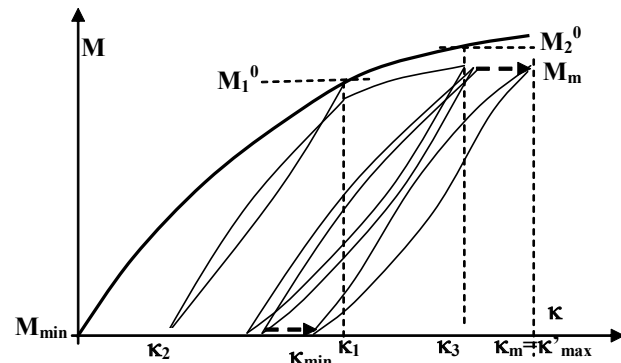
Fig. 1. Coordinate systems of relationship M – κ

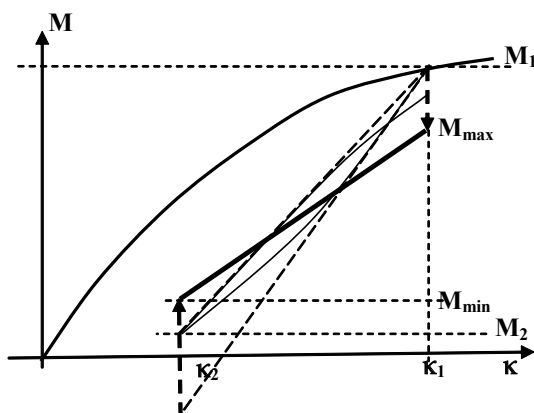Fig. 2. Scheme relationship M(κ) for changing loads
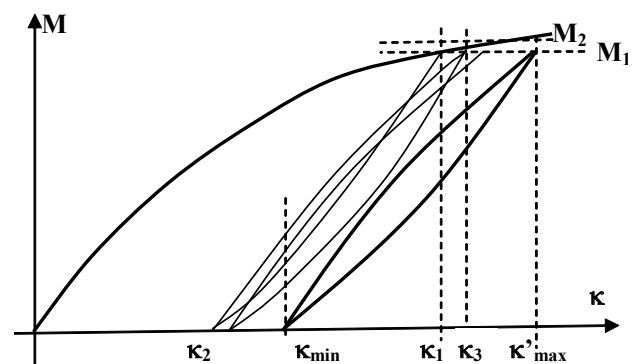

Fig. 3. Deformation hysteresis loop
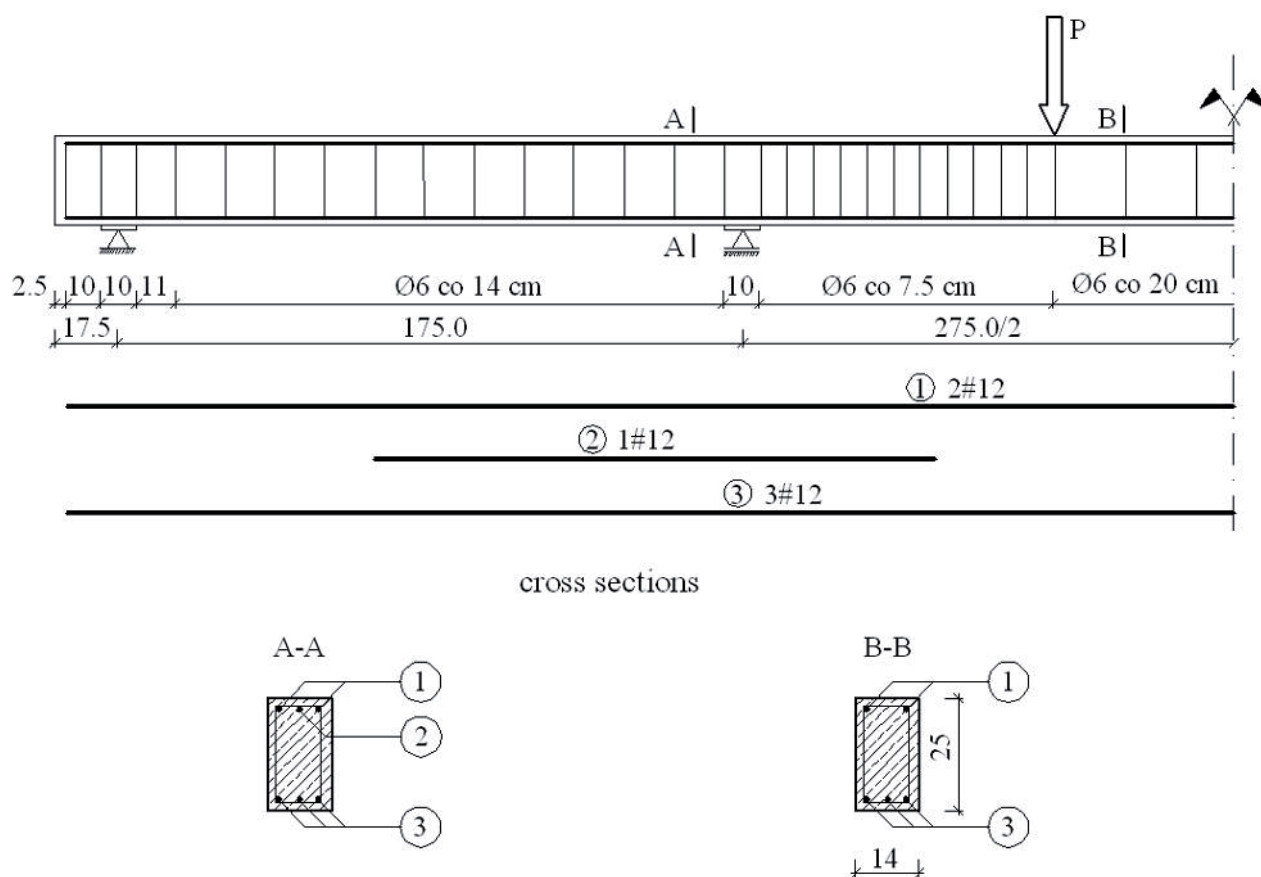

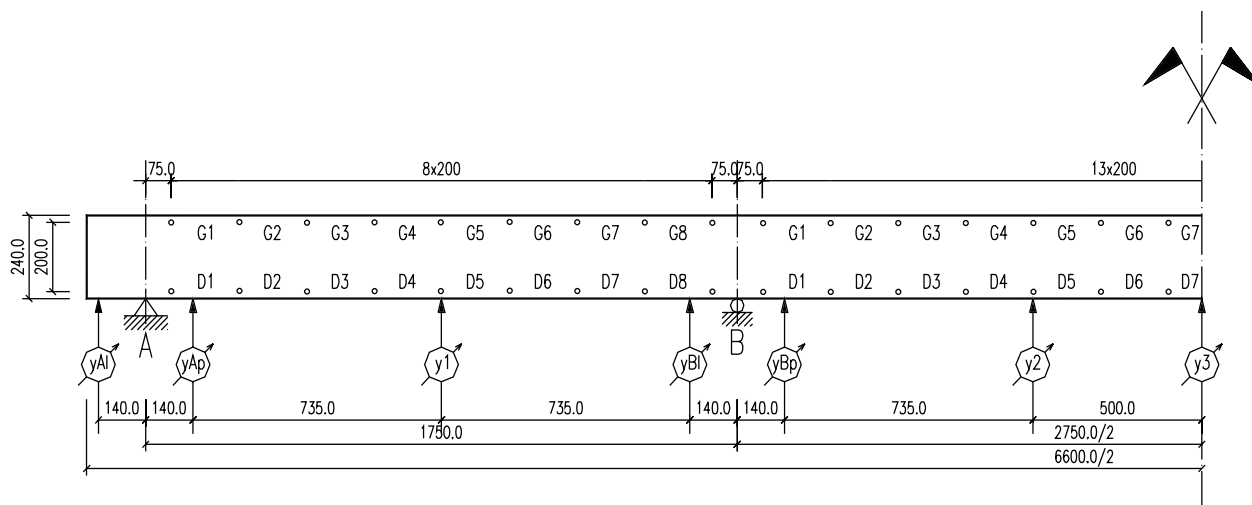Fig. 4. Moment hysteresis loop

Fig. 5. Static scheme, beam reinforcement

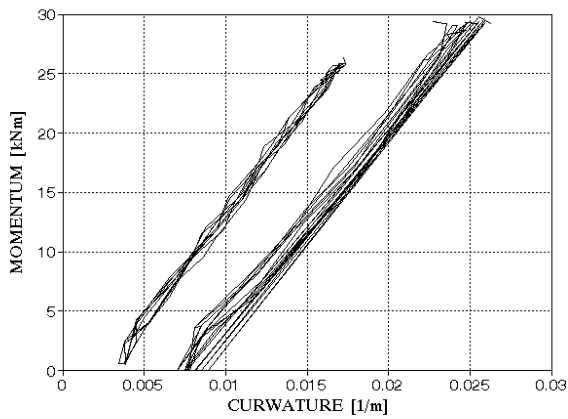Fig. 6. Distribution of measuring points of deflection and deformation basis
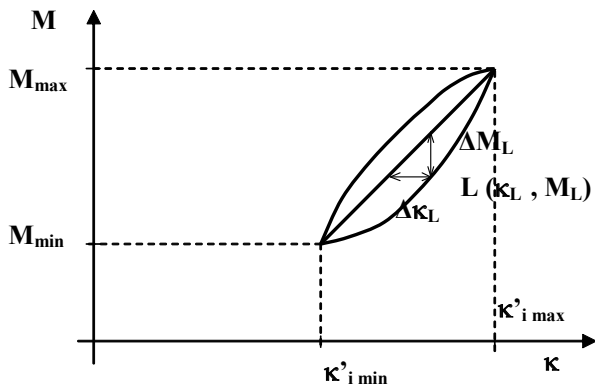
Fig. 7. Example two series of moment loops M(κ)

Fig. 8. Distance from the empirical point 'L' of the loop
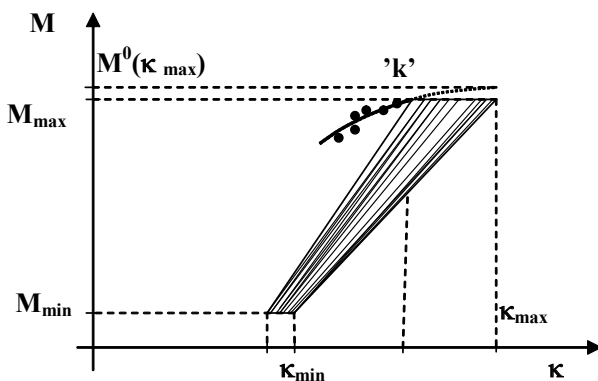*M*(κ) from the linearised form

Fig. 9. Linearisation of load and unload branches of
relationship *M*(κ)

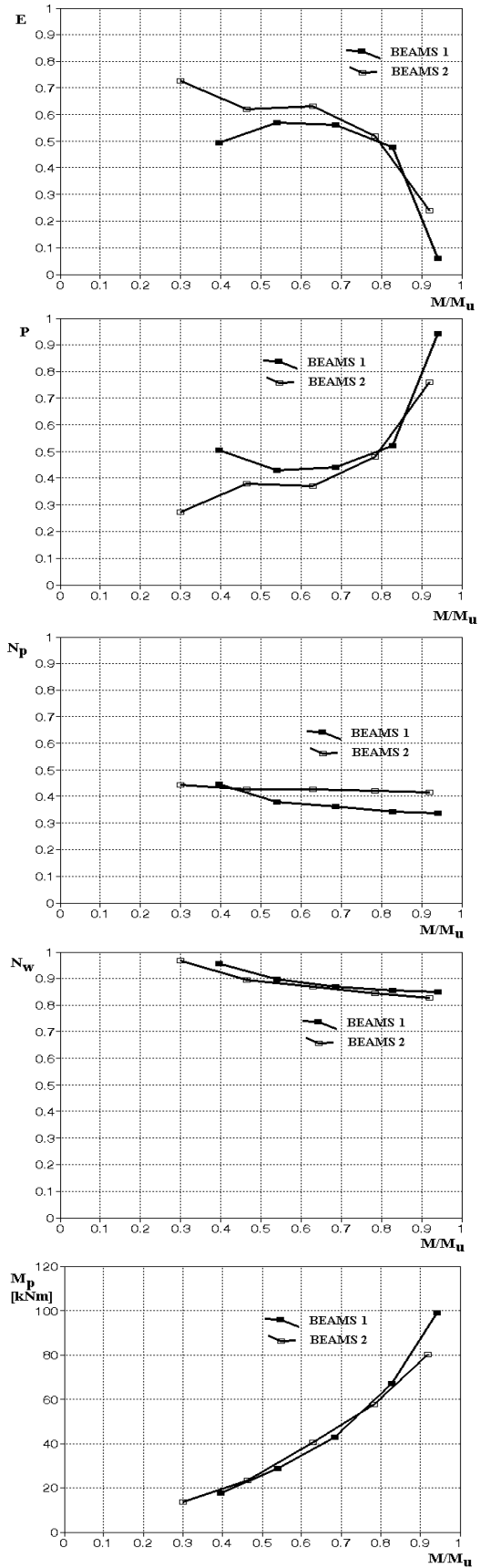Fig. 10. The course of average values *E*, *P*, N_p, N_w, M_p in
the function of effort M/M$_u$

Zależność M(κ) na podstawie wyników badań belek poddanych obciążeniom zmiennym

Jacek Śluszrczyk

1. Wstęp

Przy obliczaniu konstrukcji żelbetowych szczególne znaczenie ma relacja moment - krzywizna $M(\kappa)$. Zależność ta decyduje o dystrybucji sił wewnętrznych w ustrojach statycznie niewyznaczalnych oraz o wielkościach ugięć elementów. W rzeczywistych warunkach eksploatacyjnych, konstrukcja żelbetowa poddawana jest nie tylko obciążeniom narastającym ale i odciążeniom.

W elementach zginanych wykonanie nawet kilku cykli statycznych obciążeń i odciążeń wywołuje przyrost ugięć doraźnych. Budowa jednolitego modelu zależności $M(\kappa)$ opisującego cały zakres od stanu sprężystego do pełnego uplastycznienia z uwzględnieniem obciążeń powtarzalnych (pętli histerezy) wymaga przeprowadzenia odpowiednich badań.

2. Model przekroju

Degradacja sztywności przekroju jest wynikiem procesów niszczenia i uplastycznienia. Jednolity opis procesów zachodzących w przekroju belki żelbetowej można uzyskać wykorzystując prawdopodobieństwa pracy sprężystej, plastycznej oraz niszczenia, odniesionych do sztywności przekroju. Podczas obciążania, rośnie stopień (prawdopodobieństwo) uplastycznienia i zniszczenia przekroju, przy czym można przyjąć dla uproszczenia, że procesy te od siebie nie zależą. W trakcie odciążania, w części uplastycznionej strefy przekroju, powstają naprężenia przeciwnych znaków dodatkowo degradujące sztywność. Również w tym wypadku można postulować niezależność procesów niszczenia i uplastycznienia, ale prawdopodobieństwa określające zaawansowanie tych procesów są prawdopodobieństwami warunkowymi zależnymi od stopnia uplastycznienia przekroju podczas obciążania. Wykorzystując przyjęte założenia, funkcję $M'_i(\kappa_i')$ dla i – tej gałęzi można opisać wzorem

$$M'_i = (B_0\, \kappa'_i\, E_i + P_i\, M_{p\,i})\, N_{p\,i}\, N_{w\,i}, \tag{1}$$

gdzie:

B$_0$ – sztywność przekroju w fazie Ia,

i – numer przedziału obciążania,

κ'_i – bezwzględna wielkość przyrostu krzywizny,

E_i, P_i – funkcje prawdopodobieństwa pracy sprężystej i plastycznej,

M_{pi} – funkcja wielkości momentu przenoszonego przez przekrój uplastyczniony,

$N_{p\,i} = N_{p\,1} - R_{p\,i}$ – funkcja prawdopodobieństwa niezniszczenia obciążeniem

$N_{w\,i} = N_{w\,1} - R_{w\,i}$ – funkcja prawdopodobieństwa niezniszczenia przekroju odciążeniem

$R_{p\,i}$ – funkcja prawdopodobieństwa zniszczenia obciążeniem

$R_{w\,i}$ – funkcja prawdopodobieństwa zniszczenia przekroju odciążeniem

Ponieważ wszystkie funkcje wyróżnione pogrubioną kursywą zależą od przyrostu krzywizny, w zapisach pominięto wskazanie odciętych.

W przypadku monotonicznych funkcji prawdopodobieństw, poszczególne gałęzie są również funkcjami monotonicznymi i przedstawiony schematycznie na rys. 1 teoretyczny związek M-κ wskazuje na możliwość odwzorowania rzeczywistego przebiegu tej zależności.

3. Wyznaczenie wartości funkcji modelowych na podstawie badań doświadczalnych.

Doświadczalne poznanie pracy przekroju i elementu pod obciążeniem doraźnym (bez efektów dynamicznych) z uwzględnieniem odciążeń przeprowadzono na trzech trójprzęsłowych belkach żelbetowych (BELKA1, BELKA 2, BELKA 3). Przebieg wyznaczonych wartości funkcji modelowych E, P, N_p, N_w, M_p w funkcji wytężenia m = M/M$_u$ (M$_u$ - empiryczny moment niszczący) przedstawiono graficznie na rys. 10.

4. Podsumowanie

W zakresie obciążeń do ~0.9 momentu niszczącego wpływ odciążeń na zachowanie się belek żelbetowych jest niewielki, obserwuje się jedynie przyrost niszczenia sztywności przekroju o ~15-18%. Proces niszczenia podczas obciążania jest znaczny gdyż dla wytężeń ~0.9 prawdopodobieństwo zniszczenia

sztywności przekroju wynosi 59-66%. Prawdopodobieństwo uplastycznienia przekroju osiąga w badanym zakresie obciążeń wartość 65-80%. W zakresie obciążeń do ~0.70 M_u obserwuje się niewielki wzrost prawdopodobieństwa pracy sprężystej o ~0.03-0.08% co wskazuje na większą koncentrację niszczenia w uplastycznionych częściach przekroju.

W zastosowaniach praktycznych pętle histerezy w procesie obciążeń zmiennych można linearyzować. Kąt nachylenia prostej zależy jedynie od iloczynu wartości prawdopodobieństw niezniszczenia $N_{pk}\,N_{wk}$.

MARIA WŁODARCZYK

Kielce University of Technology,
Al. Tysiąclecia Państwa Polskiego 7,
25-314 Kielce, Poland,
e-mail: mariaw@tu.kielce.pl

CRACKING PROCESS OF REINFORCED CONCRETE BEAMS IN FUNCTION OF BENDING MOMENT

Abstract

The results of performed test on reinforced concrete beams were treated as the basis for the further analysis. The beams differed only in the way of load application. Below the value of nominal cracking moments the growth of process intensity is very small and above it can be regarded as proportional to the bending moment. The process intensity λ for the beams subjected to live load comparing to the beams under monotonous load grows faster with the increasing load.

Keywords: bending moment, reinforced concrete beams

1. Introduction

The stochastic model of the process of crack formation and their calculation method in the reinforced concrete elements is described in the paper [1]. The distance between cracks was calculated assuming that close to the crack location loss of the adherence between concrete and steel occurs and stresses in concrete decrease. This excludes forming of a new crack on the left- (a_L) and right-side (a_P) of the developed crack. Using this model a computer programme to estimate the intensity of cracking process has been written [2].

In the paper an attempt to estimate relations between the intensity of cracking process and bending moment has been done. The results of performed test on reinforced concrete beams were treated as the basis for the further analysis. The beams differed only in the way of load application.

2. Description of the experiments

The experimental tests was performed on simply supported beams using the so-called four-point bending loading. There is a zone of pure bending in the beam tested. The section was monitored carefully for getting reliable data about strain localization and crack width for different levels of loading and unloading. In the following, a detailed description of examined reinforced concrete beams is given.

Two series of technically identical, reinforced concrete beams differently loaded were examined.

The first series of examined beams consisted of four reinforced beams and the second series consisted of 13 beams. For all the tested beams the tension zone was reinforced with three bars ϕ12 made of steel 34GS, with mean yield strength of reinforcement f_{yk} = 435,23 MPa. In the compression zone two bars ϕ 8 made of steel St3S were used. For stirrups ϕ4,5 bars made of St3S steel were used. Between the applied forces 225 mm stirrup spacing, whereas 100 mm stirrup spacing at the supports was used.

Beams were made of concrete of identical recipe. Mean value of concrete compressive strength was estimated on the basis of experimental data and varied from f_{cm} = 22.08 MPa to f_{cm} = 29.56 MPa for each batches of concrete.

The beams of the first series (S1) were subjected to step growing load: $0 \rightarrow 5 \rightarrow 7,5 \rightarrow 10 \rightarrow 15 \rightarrow 20 \rightarrow 25$ kN and so on, until collapse. The beams of second series (S2) were subjected to step live load with repeated unloading on higher load level: $0 \rightarrow 5 \rightarrow 7,5 \rightarrow 10 \rightarrow 0 \rightarrow 10' \rightarrow 15 \rightarrow 0 \rightarrow 15' \rightarrow 20 \rightarrow 0 \rightarrow 20' \rightarrow 25$ kN and so on, till collapse. Load capacity force for beams ranged from 34.75 kN up to 38.75 kN.

For each loading and unloading analysed, on the surface of concrete at the level of tensile reinforcement, measurements of crack width and their location were carried out. The test results of two series of reinforced concrete beams were written into the data bases and were used for further analysis.
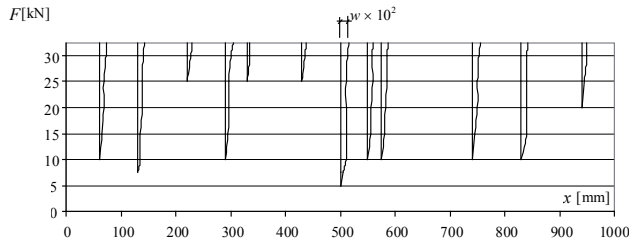
3. The results of research

Fig. 1. Process of crack forming in S1B01 beam

Graphical method of presentation of the test results was used because of the size of digital data bases developed. The test results are illustrated, as an example, for S1B01 beam (Fig. 1) and for S2B01 beam (Fig. 2).
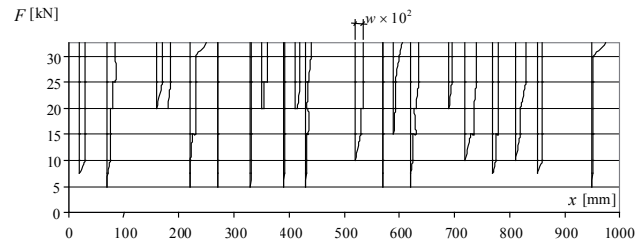

Fig. 2. Process of crack forming in S2B01 beam

Mean distances between cracks for each tested beams are given in the table 1.

Table 1. Mean, experimental distances between cracks

Beam	Mean distances between cracks x [mm] for tested beams on each level of load F [kN]												
	7,5	10	10'	15	15'	20	20'	25	25'	30	30'	32.5	35
S1B01	408	241	–	124	–	117	–	105	–	91	–	84	–
S1B02	261	190	–	128	–	108	–	93	–	85	–	–	80
S1B03	1000	426	–	317	–	175	–	140	–	96	–	88	84
S1B04	310	213	–	150	–	108	–	98	–	86	–	80	80
S2B01	1000	243	243	192	173	121	113	101	101	101	91	91	–
S2B02	-	512	512	205	205	249	249	181	181	149	140	133	26
S2B03	1000	174	179	110	088	82	75	64	64	64	64	63	–
S2B04	1000	476	227	122	116	78	68	66	64	60	60	60	–
S2B05	1000	255	289	224	146	108	85	76	73	71	71	–	–
S2B06	146	113	107	89	89	85	78	76	68	66	66	–	–
S2B07	1000	208	122	104	86	69	67	63	63	61	61	59	–
S2B08	194	164	118	89	85	85	85	85	82	79	79	–	–
S2B09	–	517	344	167	187	131	111	111	95	91	84	–	–
S2B10	1000	305	244	202	187	162	151	122	104	96	92	92	89
S2B11	–	511	633	156	137	115	115	109	99	91	87	70	70
S2B12	210	175	293	155	155	127	127	115	79	79	74	71	71
S2B13	–	–	507	197	181	151	141	132	85	85	85	85	–

4. The intensity of cracking process

In order to describe the intensity of cracking process λ the probabilistic model of crack formation proposed in [3] was used. The governing equation is:

$$\frac{\delta f_\lambda(\lambda,t)}{\delta\lambda} =$$ (1)

$$= \begin{cases} -f_\lambda(\lambda,t)\int_{2a}^{\infty} z_c f_\lambda(\lambda,t)dz & \text{for } t \le 2a \\ -f_\lambda(\lambda,t)\int_{2a}^{\infty} z_c f_\lambda(\lambda,t)dz + 2\int_{t+2a}^{\infty} f_\lambda(\lambda,t)dz & \text{for } a \le t < 2a \\ -f_\lambda(\lambda,t)\int_{2a}^{\infty} z_c f_\lambda(\lambda,t)dz + 2\int_{t+2a}^{\infty} f_\lambda(\lambda,t)dz - t_c f_\lambda(\lambda,t) & \text{for } t \ge 2a \end{cases}$$

where: a is the length of section where loss of adherence between concrete and reinforcement occurs, λ is the intensity of cracking process.

The solution of (1) was obtained numerically using programme LAMBDA [2] written for this purpose.

The length of adherence loss section a was estimated on the basis of the measured crack width and the value of stresses in reinforcement at the crack location:

$$a = \frac{wE_s}{2\sigma_{IIa}}$$ (2)

where: w is the width of crack, E_s is the elasticity modulus of reinforcement, and σ_{IIa} is the stress in reinforcement at the crack location.

In case of overlapping adherence loss sections (Fig. 3) the value of a was calculated using the following relation:

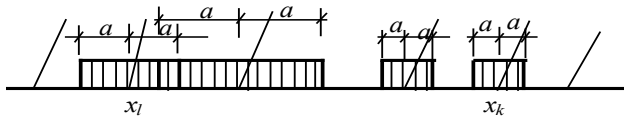$$2a + x_l - x_k = \sum_{k=1}^{l} \frac{w_i E_s}{2\sigma_{IIa}}$$ (3)

Fig. 3. Overlapping adherence loss sections

Since the process of calculation had to be repeated several times, where a is a variable, a tool programme ODCINEK_A [2] was developed.

Because of random character of adherence loss section the parameter a was defined as a random variable. The length of adherence loss section is then treated as an independent random variable for a given type of beam with probability density function $f_a(a)$ and mean value $E(a)$. As a result the following equation for random function is obtained:

$$f(x,\lambda) = \int_0^\infty f_a(a) f_\lambda(x|a)\, \mathrm{d}a \qquad (4)$$

To calculate the random function with a treated as a random variable [3], programme ROZSTAW [2] was used. The result being the probability density functions $f(x,\lambda)$ are presented in Fig. 4, and relation between mean distances of cracks and the process intensity in Fig. 5.
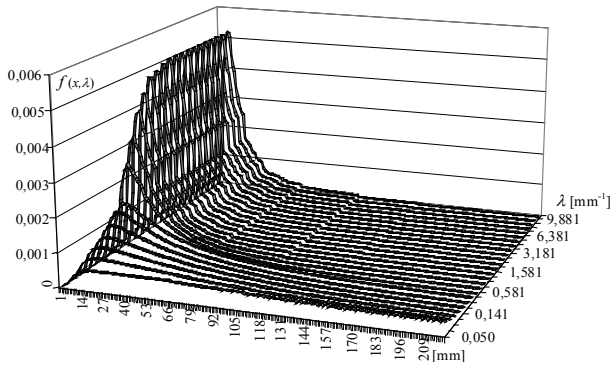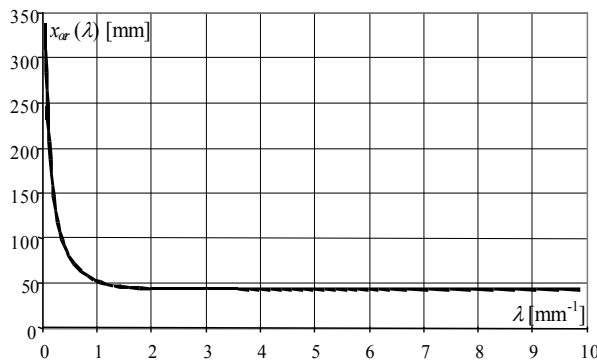

Fig. 4. Density function

Fig. 5. Theoretical relationship between the mean distance of crack and the intensity process

5. Relationship between the intensity of crack process and bending moment

In order to determine the relation between the intensity process function λ and the bending moment mean theoretical values of crack distances have been adjusted to the experimental distances for each beam:

$$x_{sr,j}\left(M_j\right) = x_{sr}\left(\lambda_{i,j}\right) \qquad (5)$$

where: i is the number of beam, j is the load number of load.
Hence, the empirical values of the function were estimated:

$$\lambda_{i,j} = \left(M_j\right) \qquad (6)$$

and shown in Fig. 6.

For theoretical description the relation $\lambda(M)$ the polynomial function was applied. Polynomials up to third degree have been analysed in case of the monotonously and low–cyclically loaded beams.

Approximating function parameters have been determined using the least square method by minimizing the distance:

$$S^2 = \sum_{i=1}^{n} \sum_{j=1}^{m} \left[\lambda_{i,j} - \lambda_{i,j}\left(M_{i,j}\right)\right] \qquad (7)$$

where: $\lambda_{i,j}$ is the value for beam i and load j.

Values determined from (7) are presented in the Table 2.

Since the deviation squares S^2 in case of linear or parabolic functions do not differ significantly, then, linear function can be accepted without loss of approximation accuracy. Finally, for linear approximating functions results are presented in Fig. 6.
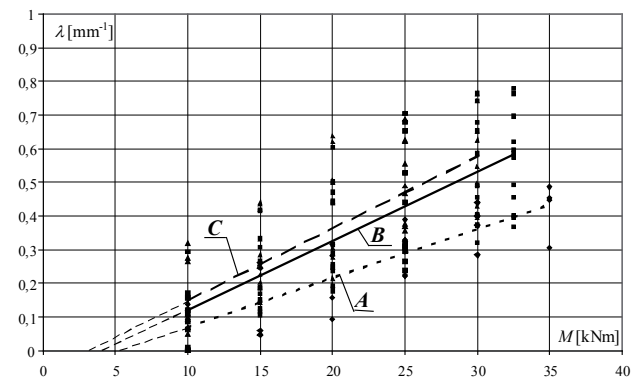
Fig. 6. Relationship $\lambda(M)$ for investigated beams

In Fig. 6 rhombuses mark quantities results for beams from the first series and a dotted line the corresponding approximation function A. Square and triangle marks

37

Table 2. Approximating function parameters and deviations

Function	a	b	c	d	S^2
The first series (monotonic load)					
$\lambda(M) = aM+b$	0,0146	-0,0776	–	–	0,0005
$\lambda(M) = aM^2 +bM+c$	-0,00009	0,0187	-0,1166	–	0,0003
$\lambda(M) = aM^3+bM^2 +cM+d$	-0,00003	0,0001	0,0142	-0,0893	0,0016
Second series (primary load)					
$\lambda(M) = aM+b$	0,0204	-0,0839	–	–	0,0016
$\lambda(M) = aM^2 +bM+c$	-0,0003	0,0345	-0,2134	–	0,0021
$\lambda(M) = aM^3+bM^2 +cM+d$	0,000004	-0,0006	0,0390	-0,2399	0,0024
Second series (secondary load)					
$\lambda(M) = aM+b$	0,0215	-0,0686	–	–	0,0031
$\lambda(M) = aM^2 +bM+c$	-0,0006	0,0442	-0,2674	–	0,0019
$\lambda(M) = aM^3+bM^2 +cM+d$	-0,00004	0,0015	0,0051	-0,0462	0,0417

are given for the beams from the second series. For the path of the primary loading squares are used with a corresponding function marked with a solid line **B**, whereas for the secondary loading path triangles are used with the corresponding broken line **C**.

In the modelling, the cracking moment for the tested beams corresponds to the process intensity, for which mean crack distance is $x_{śr} = 1000$ mm. Since the description of the process for large distances between cracks is almost identical with classic Poisson's process, the obtained value:

$$\lambda_{cr} \approx \frac{1}{x_{śr}} = \frac{1}{1000} \ [\text{mm-1}], \qquad (8)$$

is close to zero. It can be accepted that the extrapolation of the lines (thin broken lines) until intersection with moment axis determine values of the nominal cracking moments:

$$M_{cr} = -\frac{b}{a} \qquad (9)$$

Using (9) the value of nominal cracking moment for the beams in the first series is $M_{cr} = 5,31$ kNm. For the beams in the second series subjected to live load the value for the primary load path is $M_{cr} = 4,11$ kNm, and on the secondary load path is $M_{cr} = 3,19$ kNm.

Value of cracking moment calculated according to the norm [5] is equal to $M_{cr\,tot} = 9,36$ kNm and is significantly higher not only than nominal cracking moments but also then ones observed during the tests (Table 1).

Comparing the quantities of nominal cracking moments it has been concluded that for the beams for the second series moments are smaller than for the first series. The lower values are the result of live load influence.

Analysing the relations $\lambda(M)$ (Fig. 6) the differences in the position of approximating functions are noticeable. The significant influence of live load on the increase in the process intensity is visible (lines **B** and **C**) in relation to the monotonously loaded beams (line **A**).

For live loads lines **B** and **C** are similar. Values $\lambda(M)$ for the secondary load (line **C**) are above the values obtained on the increasing path, which is the result of cumulating influence of live loads.

The differences between **B** and **C** lines come from adding the effect of the last unload. These differences grow along with the unload value.

It has also been observed that the faster growth of process intensity begins above nominal cracking moments.

6. Conclusions

1. Below the value of nominal cracking moments the growth of process intensity is very small and above it can be regarded as proportional to the bending moment.
2. A significant influence of live load on quantities of nominal cracking moments has been observed.
3. The process intensity λ for the beams subjected to live load comparing to the beams under monotonous load grows faster with the increasing load.

References

[1] Goszczyński S., Goszczyńska B.: *Losowy proces tworzenia się rys w belkach żelbetowych*. Archiwum Inżynierii Lądowej, Tom XXVI 3 (1980), s. 603 – 620.

[2] Włodarczyk M.: *Zarysowanie zginanych belek żelbetowych jako proces stochastyczny*. Praca doktorska. Kielce 2002.

[3] Goszczyńska B.: *Losowy proces powstawania rys w strefie czystego zginania belek żelbetowych*. Praca doktorska. Kielce 1984.

[4] Goszczyński S., Włodarczyk M.: *Wpływ średnicy zbrojenia na wielkość odcinka utraty przyczepności*. XLVII Konferencja Naukowa KILiW PAN i KN PZITB, Krynica 2001, s. 83-90.

[5] PN-B-03264:2002, *Konstrukcje betonowe, żelbetowe i sprężone. Obliczenia statyczne i projektowanie*.

structure
structure

Maria Włodarczyk

Proces zarysowania belek żelbetowych w funkcji momentu zginającego

1. Wstęp

Stochastyczny model procesu powstawania rys w elementach żelbetowych oraz metodę ich obliczania został zaproponowany w pracy [1]. Obliczanie rozstawu rys oparto na założeniu, że w otoczeniu powstałej rysy następuje zerwanie przyczepności pomiędzy betonem i stalą oraz spadek naprężeń w betonie, co wyklucza powstanie nowej rysy w jej lewo- (a_L) i prawostronnym (a_P) otoczeniu. W prezentowanej pracy podjęto próbę oszacowania relacji między intensywnością procesu zarysowania i momentem zginającym.

2. Opis przeprowadzonych badań

Zbadano dwie serie, identycznych technicznie, belek żelbetowych różniących się między sobą sposobem realizacji obciążenia. Dla wszystkich zbadanych belek w strefie rozciąganej zastosowano trzy pręty φ12 ze stali 34GS o średniej granicy plastyczności f_{yk} = 435,23 MPa i w strefie ściskanej dwa pręty φ8 ze stali St3S. Belki wykonano z betonu o takiej samej recepturze. Średnia wytrzymałość określona na podstawie wyników badań wahała się od f_{cm} = 22,08 MPa do f_{cm} = 29,56 MPa dla poszczególnych zarobów.

Wszystkie badane belki były swobodnie podparte i obciążone dwoma siłami skupionymi w odległości $l/3$ od podpór. Pierwsza seria belek (S1) była poddana działaniu obciążenia skokowe, narastającego aż do zniszczenia. Natomiast drugą serię belek (S2) poddano działaniu obciążenia złożonego, które obejmowało skokowy wzrost siły z kilkukrotnymi odciążeniami. Siła niszcząca wahała się od 34,75 kN do 38,75 kN.

Na poszczególnych poziomach obciążenia i odciążenia wykonano między innymi pomiary szerokości rys oraz zinwentaryzowano ich położenie. Pomiary były prowadzone na powierzchni betonu w miejscu występowania zbrojenia rozciąganego.

3. Wyniki badań

Ze względu na duże rozmiary baz do prezentacji uzyskanych wyników zastosowano metody graficzne. Rezultaty uzyskane z badań poszczególnych be-lek zostały przykładowo zilustrowane wynikami dla belki S1B01 (rys. 1) i dla belki S2B01 (rys. 2).

4. Intensywność procesu zarysowania

W celu opisania intensywności procesu zarysowania λ wykorzystano zaproponowany w [1] probabilistyczny model powstawania rys. Rozwiązanie równania:

$$\frac{\delta f_\lambda(\lambda,t)}{\delta\lambda} = \qquad (1)$$

$$= \begin{cases} -f_\lambda(\lambda,t)\int\limits_{2a}^{\infty} z_c f_\lambda(\lambda,t)dz & \text{dla } t \leq 2a \\[2ex] -f_\lambda(\lambda,t)\int\limits_{2a}^{\infty} z_c f_\lambda(\lambda,t)dz + 2\int\limits_{t+2a}^{\infty} f_\lambda(\lambda,t)dz & \text{dla } a \leq t < 2a \\[2ex] -f_\lambda(\lambda,t)\int\limits_{2a}^{\infty} z_c f_\lambda(\lambda,t)dz + 2\int\limits_{t+2a}^{\infty} f_\lambda(\lambda,t)dz - t_c f_\lambda(\lambda,t) & \text{dla } t \geq 2a \end{cases}$$

gdzie: a – długość odcinka utraty przyczepności pomiędzy betonem i stalą, λ – intensywność procesu zarysowania.

Otrzymano na drodze numerycznej wykorzystując specjalnie napisany do tego celu program LAMBDA [2].

Długość odcinka utraty przyczepności a oszacowano na podstawie pomierzonej szerokości rysy i wielkości naprężeń w stali w przekroju przez rysę:

$$a = \frac{wE_s}{2\sigma_{IIa}} \qquad (2)$$

gdzie: w – szerokość rysy, E_s – moduł sprężystości stali, σ_{IIa} – naprężenia w stali w przekroju przez rysę.

5. Zależność pomiędzy intensywnością procesu I a momentem zginającym

W celu wyznaczenia zależności pomiędzy intensywnością procesu λ a momentem zginającym porównano średnie teoretyczne wartości rozstawu rys z odległościami doświadczalnymi dla poszczególnych belek:

$$x_{śr,i}(M_j) = x_{śr}(\lambda_{i,j}) \qquad (3)$$

gdzie: i – numer belki, j – numer obciążenia.

Na tej podstawie otrzymano empiryczne wartości funkcji

$$\lambda_{i,j}(M_j) \qquad (4)$$

Celem uzyskania opisu teoretycznego przyjęto związek $\lambda(M)$ w formie funkcji wielomianowej.

6. Wnioski

1. Do umownych momentów rysujących wzrost intensywności procesu zarysowania jest bardzo mały, a powyżej można przyjąć, że jest proporcjonalny do momentu zginającego.

2. Stwierdzono znaczący wpływ obciążeń zmiennych na wielkości umownych momentów rysujących.

3. Intensywność procesu λ dla belek poddanych obciążeniu zmiennemu w porównaniu z belkami obciążonymi monotonicznie rośnie szybciej w miarę wzrostu obciążenia.

environment
environment

EWA ZENDER-ŚWIERCZ[1]
JERZY ZB. PIOTROWSKI[2]

Kielce University of Technology,
Al. Tysiąclecia Państwa Polskiego 7,
25-314 Kielce, Poland,
[1] e-mail: ezender@tu.kielce.pl
[2] e-mail: jzpiotr@tu.kielce.pl

ELIMINATION OF THE NEGATIVE INFLUENCE OF TIGHT BUILDING STRUCTURE ON VENTILATION

A b s t r a c t

Ventilation of accomodation in warmed buildings well with tight windows' joinery is perturbed. The two-function heaters which are more and more frequently installed in the flats make up additional problem. This article presents results of reaserch on example of two apartments furnished with Individual System of Air Intake. This system causes reduction of CO2 concentration in rooms. Valus of this parameter has been under permissible valus (1000 ppm). The air humidity has decreased what causes reduction of the stuffy air feeling the room. In result of ventilation system action, the working of two-function water heaters has not been perturbed.

Keywords: building ventilation, tight building structure

1. Introduction

Ventilation of accommodation in warmed buildings well with tight windows' joinery is perturbed. Inhabitants complain about feeling the stuffy air in that kind of buildings. The reverse drafts are formed on the last stores. That causes the impression of drafts in periods fall – winter.

Previous research over the ventilation problems have shown, that the situation is serious because of crossing of permissible value of CO concentration. It creates threat to residents' life. Research results in detail have been described in publication [3].

Article presents results of research on example of two apartments furnished with Individual System of Air Intake. The assignment of this system is improving of microclimate in rooms with the two – function water heaters. The next task of this system is correcting the functioning of ventilation system. The investigated flats are located on the penultimate and the last storey.

2. Object of research

The analysis range (cover) flats furnished with the two – function water heaters with open combustion (chamber). CO_2 concentration, internal temperature and air humidity have been measured. Additionally measurement has ranged velocity of inlet and outlet air. Investigated flats have been ventilating by Individual System of Air Intake.
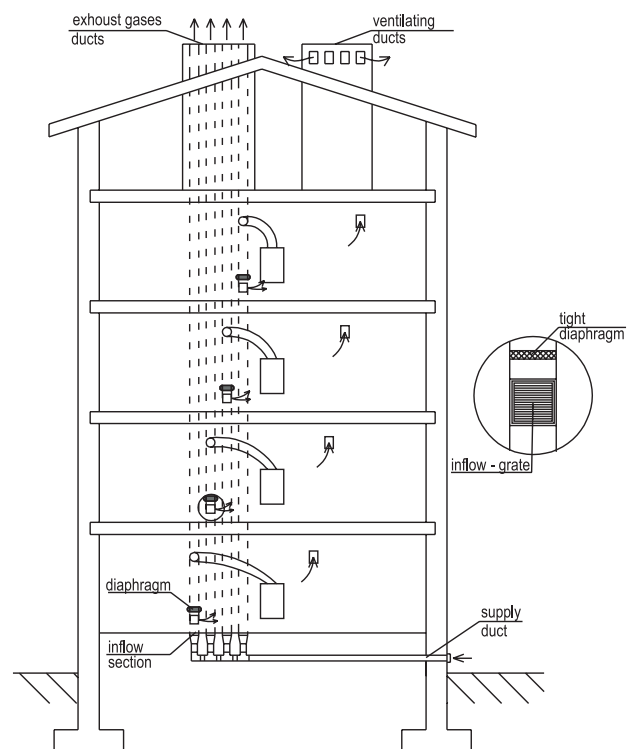

Fig. 1. Scheme of Individual System of Air Intake in building

The functioning of this system depends on supplying air to the rooms by individual ventilating ducts from level of cellar tracked. That individual ventilating

ducts are lower section of exhaust gases ducts. They are furnished with tight diaphragm which separates blowing air from exhaust gas.

Outflow – ducts are furnished with air grate situated under rooms' ceiling.

Investigation was done over the periods fall – winter. Then the mean daily temperature equaled $0,1 - 4,7^{O}C$.

The mean daily wind velocity equaled $0,7 - 4,8 \dfrac{m}{s}$.

Figure 1 shows location of the the ducts in investigated object. The inlet air is drawn from the level of cellar. Next, the air flow in the vertical ducts. Those vertical ducts are changing to combustion ducts in rooms. There is the tight diaphragm. It is located over the inlet grate which prevents from regression of the exhaust gases and flowing of those this gases into the rooms.

3. Analysis of microclimate in accommodations with the two – function water heaters with open combustion

First, the air conditions in the rooms have been analyzed. The Individual System of Air Intake has not been working. The inlet grate has been covered. Next the CO_2 concentration has been measured and compared with permissible value – 1000 ppm [2].

The results have shown that the level of CO_2 concentration has been often above the permissible value. This situation creates a/the threat to residents' life.

In next step of experiment the inlet grate was uncovered. The outlet grate was covered and uncovered respectively. The Figure 2 shows the results of this investigation.
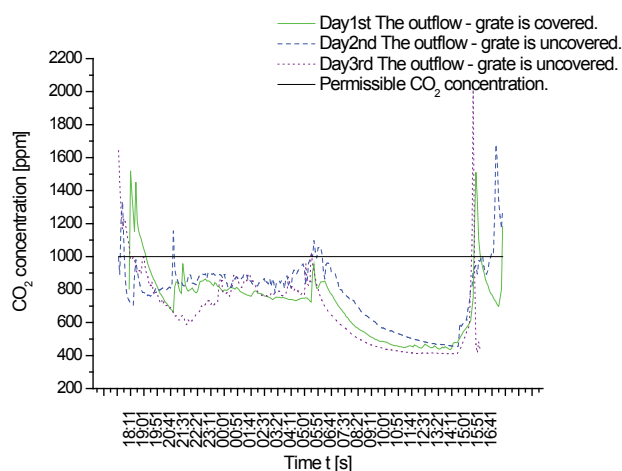

Fig. 2. Change of CO_2 concentration during normal use of accommodation at periodic switching on water heaters

CO_2 concentration has increased over permissible value during the night hours. It might be caused by

the frequently turning on the water heater because of the low temperatures outside. The measurement has been done three times. The two of them has been done when the outflow grate was uncovered, and the third one when the outflow grate was covered. Three graphs display/show the results. They are compared to each other. It implies that uncovering of outflow – grate has not effected this investigated parameter.

The next measured parameter was internal air temperature. The research results are presented in Figure 3. When the outflow grate was uncovered the average temperature in room has amounted to $21.3^{O}C$. When the outflow grate was covered the value of this parameter has increased by approximately $1^{O}C$ (from $21.3^{O}C$ to $22.2^{O}C$).
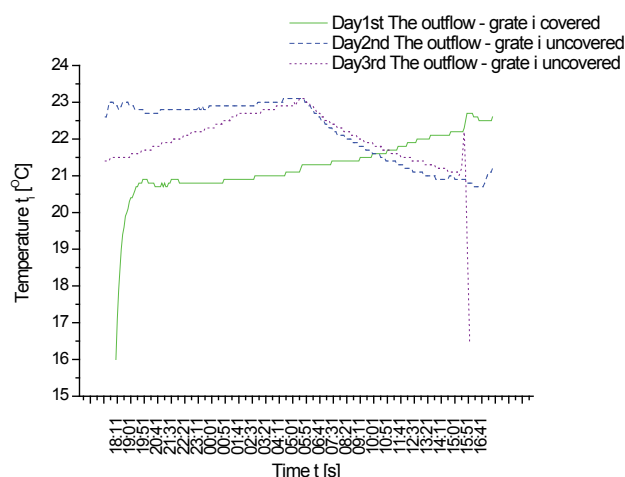

Fig. 3. Change of temperature during normal use of accommodation at periodic switching on water heaters

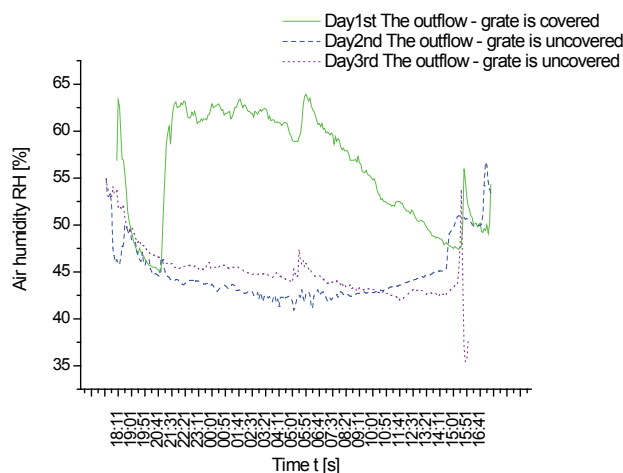The next measured parameter has been air humidity in room.

Fig. 4. Change of air humidity during normal use of accommodation at periodic switching on water heaters

The air humidity analysis has shown decrease after uncovering the outflow grate. Then the average humidity has equaled to 44.9%. When the outflow grate was covered the value of this parameter has equaled to 56%. It means that big amount of moisture run away with outlet air, but it does not cause deterioration of thermal comfort conditions.This parameter has been within range of permissible values (30-70%) [1].

The last analyzed parameter has been air velocity. It has been measured on the two last storey.

First the penultimate storey has been analyzed. During the analysis of air velocity in the duct of Individual System of Air Intake average value of this parameter has equaled $0{,}29\dfrac{m}{s}$. The outflow grate on the last storey has been covered. When the outflow grate on the last storey has been uncovered the value of average velocity has equaled $0{,}30\dfrac{m}{s}$. It means lack of influence of covering ventilation grate on the last storey on inlet air velocity on the penultimate storey. The results are presented in Fig. 5.
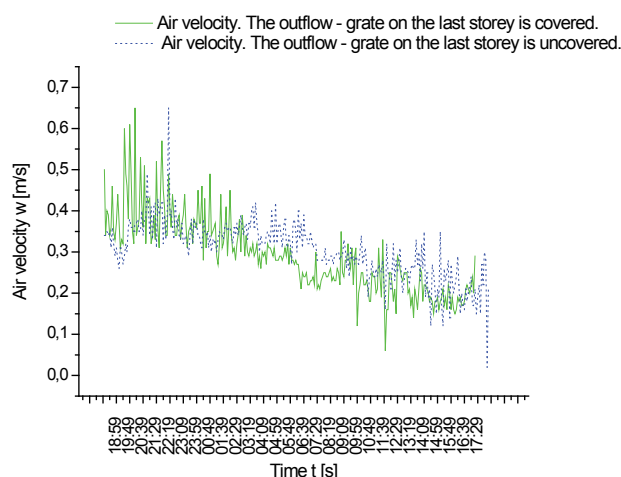
Fig. 5. Change of inlet air velocity during normal use of accommodation at periodic switching on water heaters. The penultimate storey

On the last storey there has been analyzed air velocity in the outflow grate and in the inflow grate. The average air velocity in the outflow grate has equaled $0{,}15\dfrac{m}{s}$. When the outflow grate was covered the average air velocity in the inflow grate has equaled $0{,}28\dfrac{m}{s}$. After the outflow grate was uncovered the average air velocity in the inflow grate has reduced to

the level close $0{,}21\dfrac{m}{s}$. Small velocity in the outflow duct is probably caused by the other outflow grate in the neighbouring accommodation.
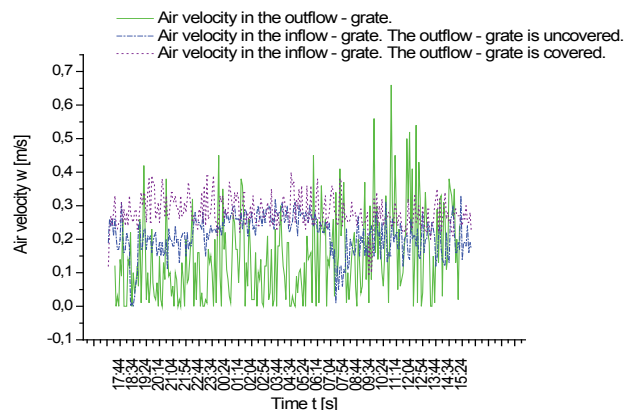
Fig. 6. Of inlet and outlet air velocity during normal use of accommodation at periodic switching on water heaters. The last storey

4. Conclusions

Using of Individual System of Air Intake holds promise on eliminating or at least reducing problems of filling discomfort in rooms with two – functions water heaters.

This system causes reducing of CO_2 concentration in rooms. Value of this parameter has been under permissible value (1000 ppm). The air humidity has decreased, what causes the reduction of stuffy air feeling inside the room.

In result of ventilation system action, the working of two – function water heaters has not been perturbed. The microclimate's conditions in room has been slightly improved.

References:

[1] PN-78 B-03421 *Wentylacja i klimatyzacja. Parametry obliczeniowe powietrza wewnętrznego w pomieszczeniach przeznaczonych do stałego przebywania ludzi.*

[2] ASHRE Standard 62, *Handbook of Fundamentals, American Society of Heating*, Refrigerating and Air-Conditioning Engineers. Inc., Atlanta 1989.

[3] Piotrowski J. Z.: *Niezbędne zmiany konstrukcyjne w przypadku montażu gazowych systemów grzewczych.* Materiały XLV Konferencji Naukowej KILiW PAN i KN PZITB. Krynica, 1999; Tom 4 Materiały budowlane konstrukcje murowe i drewniane. Fizyka budowli, s. 239-246.

Ewa Zender-Świercz, Jerzy Zb. Piotrowski

Ewa Zender-Świercz
Jerzy Zb. Piotrowski

Wyeliminowanie negatywnego wpływu szczelnej konstrukcji budynków na wentylację pomieszczeń

1. Wstęp

Dobrze ocieplone budynki, szczelna stolarka okienna powodują zaburzenia wentylacji pomieszczeń. Dodatkowy problem stanowią dwufunkcyjne podgrzewacze wody z otwartą komorą spalania, które są nadal często montowane w mieszkaniach.

2. Zakres badań

Analizie poddano kilka przykładowych obiektów. Mierzono stężenie CO_2, temperaturę i wilgotność powietrza w pomieszczeniu oraz prędkość powietrza nawiewanego i wywiewanego z pomieszczenia.

Badania prowadzone były w okresie jesienno-zimowym przy średniej dobowej temperaturze 0,1-4,7^{O}C, oraz średniej dobowej prędkości wiatru 0,7-4,8 m/s.

Mieszkania, w których przeprowadzano badania wyposażone były w indywidualny system nawiewny (ISN), gdzie kanały doprowadzające powietrze prowadzone były z poziomu piwnicy. Kanały nawiewne stanowiły dolne odcinki przewodów spalinowych. Powietrze doprowadzane do pomieszczenia oddzielała od spalin szczelna przepona (rys. 1). Kanały wywiewne prowadzone były oddzielnie i wyposażone zostały w kratkę wentylacyjną usytuowaną pod stropem pomieszczeń.

3. Analiza warunków panujących w pomieszczeniach z dwufunkcyjnymi podgrzewaczami wody

Gdy kratka nawiewna była zasłonięta poziom stężenia CO_2 przekraczał wartość dopuszczalną (1000 ppm). Oznacza to, że sytuacja taka poważnie obniżała odczuwalny komfort mikroklimatyczny w pomieszczeniu.

Po odsłonięciu kratki nawiewnej stężenie CO_2 obniżyło swą wartość do poziomu akceptowalnego.

Przy odsłoniętej kratce nawiewnej sprawdzono zachowanie się pozostałych mierzonych parametrów. Analizę przeprowadzono odsłaniając i zasłaniając kratkę wywiewną.

Odsłonięcie kratki wywiewnej spowodowało zmniejszenie wilgotności powietrza do poziomu w zakresie wartości 40-50% tzn. zawartych w przedziale dopuszczalnym (30-70%). Oznacza to, iż wilgoć w dużej mierze odbierana jest przez powietrze wywiewane.

Temperatura powietrza uległa podwyższeniu po odsłonięciu kratki wywiewnej. Błędne jest więc zasłanianie kratki wentylacyjnej przez użytkowników mieszkań.

Prędkość powietrza w kratce nawiewnej po odsłonięciu kratki wywiewnej uległa zmniejszeniu. Osiągnęła w ten sposób wartość korzystniejszą z punktu widzenia komfortu cieplnego pomieszczeń, tzn. oscylowała wokół 0,2 m/s. Użytkownicy nie odczuwali nieprzyjemnego przeciągu.

4. Wnioski

Wstępna analiza obiektów z indywidualnym systemem nawiewnym pozwala sądzić, iż takie rozwiązanie poprawi mikroklimat pomieszczeń z dwufunkcyjnymi podgrzewaczami wody.

Stężenie CO_2 zmniejszyło się poniżej wartości dopuszczalnej. Również wilgotność powietrza uległa redukcji, co spowodowało zmniejszenie odczucia duszności w pomieszczeniu.

Na uwagę zasługuje fakt, iż proponowane prowadzenie kanałów nawiewnych i wywiewnych nie zaburza działania dwufunkcyjnych podgrzewaczy wody.

MAREK TELEJKO

Kielce University of Technology,
Al. Tysiąclecia Państwa Polskiego 7,
25-314 Kielce, Poland,
e-mail: mtelejko@tu.kielce.pl

ADDITIONAL AIR INTAKES AS THE ELEMENT SUPPORTING NATURAL VENTILATION

Abstract

Enlargement of the thermal isolation of external barriers is the simplest and the most effective way to reduce the waste energy on the heating aims. Unfortunately, inappropriate analysis and luck of coordination while performing thermomodernizational work, negatively influences the microclimate in such objects. The size and the distribution of the intake openings has been decisive for proper functioning of gravitational ventilation and warranty for the proper parameters of internal microclimate. Even small works done on thermomodernizational ventilation may influence the quality of work of the whole system of gravitational ventilation. These work should be carefully designed, planned and carried out efficiently.

Keywords: natural ventilation, air intakes

1. Introduction

The growth of maintenance costs of objects and taking care of natural environment have led to searching and promoting solutions reducing the waste of energy on the heating aims of objects. Enlargement of the thermal isolation of external barriers is the simplest and the most effective solution as far as this problem is concerned. Unfortunately, inappropriate analysis and not coordinated thermomodernizational work has negative influence on the microclimate in interiors of such objects. This article presents the problems met while leading research concerning microclimatic conditions in buildings where thermo - modernization was used. Polish standards related to microclimatic conditions, ventilation of buildings and air exchange were contained in three legal acts. In the decree [1] in the matter of technical conditions which the buildings and their location should obey the general requirements concerning ventilation were presented. Moreover, detailed requirements related to individual solutions of the ventilation systems were presented in valid for about twenty years norm [2] and its supplement [3]. This norm says, that windows of the infiltration coefficient smaller than 0.3 $m^3/(mhdaPa^{2/3})$ mounted in habitable buildings of public usefulness should be equipped with the air intakes providing the right quantity of air necessary for ventilation. In case of the lack of such an air intakes, mechanical supply ventilation has to be installed in the rooms. In all other cases, the coefficient of infiltration of woodwork has to be comprised in borders 0,5-1,0 m^3 ($mhdaPa^{2/3}$). The above mentioned requirements were settled for all buildings regardless of their height, tightness of barriers or location. These regulations are used not only in case of newly built buildings, but also with reference to objects where thermo - modernization was used. These workings are very complex as they concern the works from several fields of building engineering. Unfortunately, according to valid regulations [4], some thermomodernizational works can be conducted by the users of objects without earlier coordination or permission. This has an impact on/influences/ the quality of internal microclimate and air exchange.

2. Carbon dioxide as the indicator of air quality

The relationship between the quantity of ventilating air and the concentration of carbon dioxide inside the rooms is recognized and an applied criterion for air quality valuation. The frequent occurrence of carbon dioxide in typical conditions is not dangerous. This non – toxic gas can only cause the habitants the feeling of smaller or larger discomfort, i.e. air stuffiness. In closed rooms one usually observes the growth of carbon dioxide concentration in the air coming from external and internal sources. First of all, it penetrates to the room from the outside by means of air infiltration through untightness in the lining of the building. The growing degree of industrialization causes the growth of the level of carbon dioxide concentration in the atmosphere. At present its value is between

400 – 600 ppm. Living organisms and gas devices are the source of carbon dioxide inside the rooms. Its concentration depends on organism activity and may vary for individual people depending on their diet, the body mass and the degree of fitness. Obviously, the concentration of carbon dioxide depends on the number of people inside the room, not sufficient air exchange (the decrease of oxygen concentration in the air) and intensification of combustion processes in the room (e.g.: smoking tobacco, preparing the meals). That's why carbon dioxide was chosen as the measure of microclimate quality inside considered flats.

According to Hodgson [5], the critical value of carbon dioxide concentration is 8500 ppm. The present standards for the internal air assume the admissible level of carbon dioxide concentration is on the level of 1000 ppm. This coefficient was proposed by Max von Pettenkofer in the nineteenth century [6].

Table 1. Emission of carbon dioxide for different levels of activity [7]

A type of activity	Emission of carbon dioxide [dm³/h]
Dream (motionless recumbent position)	10 - 12
Sitting position (without doing any work)	12 - 15
Sitting posture – easy office works	18 - 25
Doing work of average difficulty	32 - 44
Doing hard work	> 55

Table 2. The influence of carbon dioxide on human organisms [8]

No.	Concentration of carbon dioxide in the air [ppm]	The symptoms
1.	300 - 450	Dry external air
2.	1000	Basis for the qualification of most standards concerning the quantity of ventilating air for a single person
3.	1550 - 500	The growing feeling of stuffiness
4.	5000	Limitations concerning working posts
5.	7000 - 10000	The growth of breathing capacity
6.	15000	The appearance of metabolical stress
7.	20000	The increased frequency of breathing and headaches
8.	40000 - 52000	Carbon dioxide concentration in the air breathing out from the lungs
9.	60000 - 80000	The possibility of partial paralysis
10.	>80000	Losing of consciousness in a few minutes

3. The object of researches

The researches were conducted in a five – storied habitable building built with traditional technology. Ventilation was designed and executed as gravitational with the system of cumulative ducts. Inside the flats there were installed gas ranges and the heaters of warm water with open combustion chamber powered with the earth gas from the grid. The buildings had external walls warmed with foamed polystyrene covered with thin – layered mineral plaster. Additionally, the users of particular flats exchanged the old window woodwork for the new one, which the infiltration coefficient spanned 0.30 – 0.45 m3/mhdaPa$^{2/3}$ (according to producer's data, depending on the flat). The object of researches were typical parameters of internal microclimate. That is, the temperature, relative humidity and concentration of the dioxide inside considered flats. Moreover, temporary speeds of the air flow and the direction of the flow of stream of air were measured through the entire period of investigation.

4. The results of measurements

During the researches there have been observed considerable disorders in performance of the system of gravitational ventilation. They mostly relied on the appearance of backward ducts in ventilating ducts. It was a principle in the considered building, that one of the ducts in the grounds of the given flat took over the part of the element delivering external air. Observed speeds near the given inlets of ventilating ducts oscillated between 0.00 m/s and 1.35 m/s for ducts removing the air. However, in case of ducts where intake ventilation took place they oscillated between 0,00 m/s and 1.44 m/s (Fig. 1). The above situation was inconvenient, because when the temperature reached approximately -10$^{\mathrm{O}}$C, the temperature of the intake air near the grate outlet equaled about +15$^{\mathrm{O}}$C (Fig. 2). In rooms in which there were air grates and air ventilation, the temperature inside the room equaled about +17 – +19$^{\mathrm{O}}$C with turned on heating. Characteristic phenomenon was the alternating character of the direction of ventilating air in particular ducts in the examined flat (Fig. 1). If the duct in the kitchen removed the air from the flat, the bathroom duct supplied external air. However, if the external air was forced in through the kitchen duct, the bathroom duct removed the internal air. Ventilation took place mostly through the duct in the room where gas devices were installed. Only in the situation when at least one casement was opened, both ducts were removing the air from the rooms. This phenomenon

indicated that too tight building casing unabled suitably right infiltration of external air. Thus, one of the ventilating ducts takes over the part of the element delivering external air, which is necessary for the needs of gas combustion and living conditions.
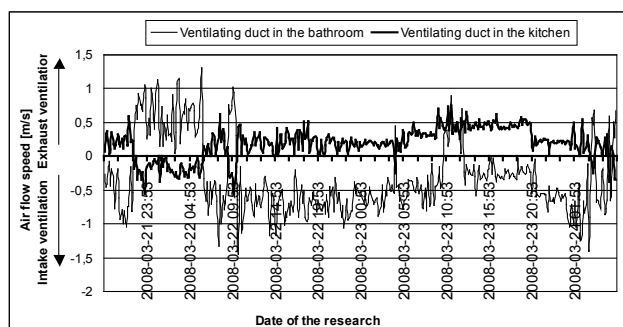

Fig. 1. The course of changeability of the direction and the speed of the stream flow of ventilating air through particular ventilation ducts
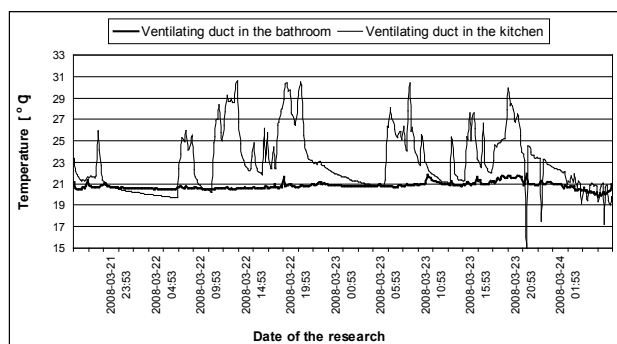

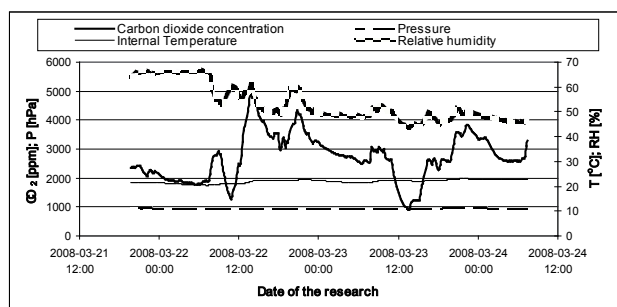Fig. 2. The diagram of changes of the temperature near the inlets of ventilating ducts

Fig. 3. The diagram of the parameters of microclimate in a chosen flat with the air inflow through the ventilating duct

The phenomenon described above influenced the level of the microclimate inside considered rooms. Carbon dioxide concentration oscillated between 2500-4000 ppm and its maximum valued equaled 5000 ppm. The concentration of carbon dioxide only fell below 2000 when the casements were opened. These values are at least twice higher compared to recommended norms. The parameter of relative humidity also achieved high values, as they oscillated between 44-68%. The diagram of internal microclimate parameters for one of the considered flats is presented in Fig. 3.

Additional air intake ventilators were installed in Additional air intake ventilators were installed in window woodwork, so as to improve internal microclimatic conditions. However, the users of flats began to complain because of too large speeds of the flow of air (causing the dry air) and cooling the rooms. Alternatively, it was proposed to bring the external air necessary for gas combustion in gas devices. This was done due to additional ducts in diameter 100 mm, bringing the air near gas stoves and heaters of warm water. The ducts were led through unused rooms, due to the fact, that the air was heated initially.
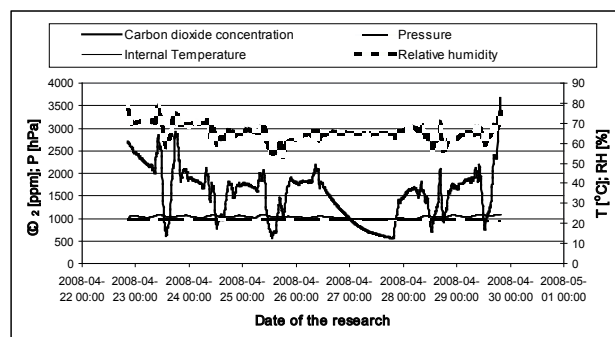

Fig. 4. The diagram of the parameters of microclimate in a chosen flat with additional intake ventilation openings

As a result of such conditions there appeared some disorders in the performance of the system of gravitational ventilation. The phenomenon of the occurrence of backward ducts in ventilating ducts and parameters describing internal microclimate accepted more reasonable values. Carbon dioxide concentration did not exceed the level 3500 ppm and the relative humidity oscillated around the value 50%. The diagram of the changeability of parameters in the flat with additional duct is presented in Fig. 4.

5. Analysis of the results. Conclusions.

The irregularities described above are the result of the limited inflow of external air to flats. That is necessary for the proper working of the ventilation system and for the proper course of the process of gas combustion in heating devices. This limitation is

the consequence of the "improvements", what limited natural infiltration of external air. All conducted works resulted in liquidation of existing paths of the inflow of external air to flats. This in turn disturbed the working of gravitational ventilation. In case of flats in which windows were not exchanged, the inflow of external air was too small. It was caused by of the lack of tightness, what caused backward ducts. Additionally, gas heating devices disturb the working of ventilation in a particular building. As a result of installing feedwater heaters with the open combustion chamber, there appeared a sudden growth of carbon dioxide concentration, with simultaneous turning back of the duct in ventilating duct. Use of the additional openings in external barriers (intake ventilators) increases the right quantity of external air. According to flat users these devices influence negatively the comfort of the use of flats. The increase of the flow of external air because of window untightness influences only an air exchange to a limited degree. Thus for the occupants it is necessary to use this function wisely. As far as window untightness is concerned, it is not possible to regulate the air stream of inflowing air. The quantity of inflowing air does not depend on internal air parameters. Additionally, quick cooling of the rooms that follows during the winter period is arduous for the flat users. Using the openings supplying the air to flats through unused rooms, significantly improved parameters of internal microclimate. However, microbiological analysis of the air is required.

To sum up the above mentioned observations it should be noticed that:

1. Disorders of microclimatic conditions in flats with tight casing and heating gas devices result in backward ducts and decrease of air exchange. However, it particularly relates to two last storeys.
2. The size and the distribution of intake openings has a decisive meaning for the proper working of gravitational ventilation and the assurances of proper parameters of internal microclimate. Each decision about the size and distribution of intake openings should be preceded with the analysis of: localizational conditions of the flat, construction al possibilities, the demand of the air (balance). The preliminary warming of ventilating air limits disorders of internal microclimate conditions.
3. Conducting thermomodernizational works, even in a small range, may influence the quality of the working of gravitational ventilation. These works should be projected and done efficiently.
4. It is possible to attain the proper working of the system of gravitational ventilation in thermo- modernized buildings under the condition of co-ordination of planned works.
5. In case of the arrangement of thermomodernizational works on several necessary years, it is necessary to settle their order, so as not to disturb the system of natural ventilation.

References:

[1] *Minister of infrastructure in the matter of technical conditions that buildings and their location should answer*. (Dz.U. Nr 75, poz. 690 with latest changes), (in polish).

[2] PN-83/B-03430 – *Ventilation in habitable buildings of collective and public usefulness*. Requirements (in polish).

[3] PN-83/B-03430:Az3:2000 – *Ventilation in habitable buildings of collective and public usefulness*. Requirements (The sheet of changes Az3), (in polish).

[4] *Act "Building Law" the seventh of July 1994* (Dz.U. Nr 156 poz. 1118 z 2006 r. with later changes).

[5] Liddament, M.W. (1996) *A Guide to Energy Efficient Ventilation*, AIVC.

[6] Nantka, M.B. (2004): *Ventilation in general construction – the review, working, problems and myths*, Materials of Installing Forum, Poznan (in polish).

[7] Fanger, P.O. (1980): *Human Comfort and Energy Consumption in Residential Buildings*, Proceedings of the International Conference on HVAC, Tucson.

[8] Sowa, J. (1995) *Migration process of the contamination in conditions of stochastic disturbances*. Doctor's thesis, Department of environmental technical university in Warsaw (in polish).

environment

Marek Telejko

Dodatkowe otwory nawiewne wspomagające wentylację naturalną

1. Wstęp
Wymagania norm krajowych.

W ciągu ostatnich 20 lat wzrosło zainteresowanie budownictwem energooszczędnym. Niestety zarówno wykonawcy, projektanci jak i przyszli użytkownicy zbyt mało uwagi poświęcają zagadnieniom wymiany powietrza, jako przedsięwzięciom drogim, nierentownym lub w ich opinii nieistotnym.

Krajowe akty prawne [3], [4], wskazują, iż okna o współczynniku a ≤ 0.3 m³/(mhdaPa²/³) montowane w budynkach mieszkalnych powinny być wyposażone w nawiewniki powietrza. Współczynnik ten ustalono dla różnicy ciśnień wynoszącej 10 Pa, bez względu na wielkość budynku czy jego usytuowanie. Analizując wymagania dotyczące szczelności stolarki okiennej w innych krajach należy stwierdzić, iż w większości z nich poza różnicą ciśnień określona jest wysokości budynku, jego szczelność lub usytuowanie. Dane te wskazują jednoznacznie, że wymagania Polskie należą do najostrzejszych.

2. Dwutlenek węgla wskaźnikiem jakości powietrza

Stężenie dwutlenku węgla wewnątrz pomieszczeń jest uznawanym i powszechnie stosowanym kryterium oceny jakości powietrza [1], [2]. Obecne standardy dla powietrza wewnętrznego zakładają dopuszczalny poziom stężenia CO_2 na poziomie 1000 ppm [1].

3. Przedmiot badań

Badania prowadzono w budynkach mieszkalnych, 3-4 kondygnacyjnych, wielorodzinnych wykonanych w technologii tradycyjnej, wybudowanych w latach 2000-2003. Obiekty wyposażone był w kanałowy system wentylacji naturalnej, kuchenki gazowe oraz piece dwufunkcyjne z otwartą komorą spalania, posiadały szczelną stolarkę okienną wyposażoną w nawiewniki oraz ściany zewnętrzne ocieplone styropianem.

4. Wyniki pomiarów

W trakcie pomiarów zanotowano bardzo duże zaburzenia w działaniu wentylacji grawitacyjnej.

W kanałach wentylacyjnych zanotowano wsteczne ciągi co w chłodne dni powodowało wyziębianie pomieszczeń. W trakcie korzystania z urządzeń gazowych odnotowano bardzo szybki wzrost stężenia CO_2. Charakterystycznym zjawiskiem był przemienny charakter przepływu strumienia powietrza wentylacyjnego w kanałach wywiewnych.

Dla poprawy mikroklimatu w mieszkaniach zaproponowano wykonanie dodatkowych otworów ϕ120 mm w ścianach zewnętrznych, a na wylotach kanałów wentylacyjnych zainstalowano urządzenia typu aspiromatic. Prace te doprowadziły do prawidłowego kierunku przepływu we wszystkich kanałach, ale jednocześnie odnotowano nadmierne wychładzanie mieszkań oraz zbyt duże prędkości przepływu.

Z uwagi na komfort użytkowników, przywrócono stan poprzedni jednocześnie wykonując otwory doprowadzające powietrze wentylacyjne w ścianach wewnętrznych na klatkę schodową i zlokalizowanych z bezpośrednim sąsiedztwie pieców gazowych. Wykres parametrów mikroklimatu w jednym z mieszkań gdzie zastosowano powyższe rozwiązania przedstawia rys. 4.

5. Analiza wyników

Zaobserwowane nieprawidłowości są wynikiem ograniczonego napływu powietrza zewnętrznego.

Zastosowanie otworów doprowadzających powietrze do mieszkań pośrednio poprzez klatkę schodową dla spalania gazu w piecach dwufunkcyjnych poprawiło parametry mikroklimatu wewnętrznego, ale wymagana jest analiza mikrobiologiczna powietrza.

6. Wnioski

1. Zaburzenia warunków mikroklimatycznych w mieszkaniach ze szczelną obudową i gazowymi urządzeniami grzewczymi przejawiają się występowaniem wstecznych ciągów oraz zmniejszeniem wymiany powietrza i dotyczą szczególnie dwóch ostatnich kondygnacjach.
2. Pojawienie się urządzenia grzewczego w mieszkaniu powinno być uzależnione od wykonania osobnego kanału, odpowiednio obudowanego,

doprowadzającego powietrze do urządzenia lub zastosowania zamkniętej komory spalania.

3. Wielkość otworów nawiewnych i ich rozmieszczenie ma decydujące znaczenie dla prawidłowego działania wentylacji grawitacyjnej oraz zapewnienia właściwych parametrów mikroklimatu wewnętrznego.

4. Decyzja o wielkości i rozmieszczeniu otworów nawiewnych powinna być poprzedzona szczegółową analizą: warunków lokalizacyjnych mieszkania, możliwości konstrukcyjnych, zapotrzebowaniem powietrza (bilans).

IWONA CISOWSKA

Kielce University of Technology,
Al. Tysiąclecia Państwa Polskiego 7,
25-314 Kielce, Poland,
e-mail: cisowska@tu.kielce.pl

STUDIES OF HYDRAULIC RESISTANCE IN POLYPROPYLENE PIPE FITTINGS

Abstract

The results of studies of local hydraulic resistance in polypropylene segmental elbows (R/d ≤ 1) and bends (R/d > 1) in systems of two or more pipe fittings connected in series are analyzed. Qualitative and quantitative formulas for the coefficient of local resistance in pipelines built from elbows and bends connected conformingly (forming spiral loops) or alternatinvely (forming sinusoidal waves) are presented.

Keywords: Pipe fittings; Pressure flow; Local resistance.

1. Introduction

The local resistance coefficients for elbows or bends found in the literature are mainly for steel or cast iron pipe fittings and they considerably differ from experimental results for single plastic pipe fittings and especially for two consecutive elbows or bends connected conformingly or alternatinvely. As yet local resistance in systems made up of several to a dozen or so elbows or bends connected in series has not been studied, so the aim of this research was to explore:
– the local resistance in systems of two or more bends or elbows conformingly connected in series to form, among others, spiral loops;
– the local resistance in systems of two or more bends or elbows alternatinvely connected in series to form, among others, sinusoidal waves.

The measurement results and physical formula for the local resistance coefficient of single segmental 90° elbows and bends was presented in dissertation (Cisowska 2004).

2. Experimental Setup

Model local resistance studies were carried out on forty six geometrical arrangements of segmental polypropylene elbows ($R/d \leq 1$) and bends ($R/d > 1$), consisting of pipe fittings with central angles $\alpha \in \{15°, 30°, 45° \text{ and } 90°\}$, relative radii of curvature $R/d \in \{1.0, 1.75, 2.25, 4.25\}$ and number of socket joints $z \in <1,48>$ at relative straight socket section length $l_k/d = 0.70$. A diagram of the experimental setup is shown in Fig. 1. The measuring lengths (0-4) were built from straight socket sections with assembly length $L_m = 1.0$ m ($L_m/d = 14.1$).
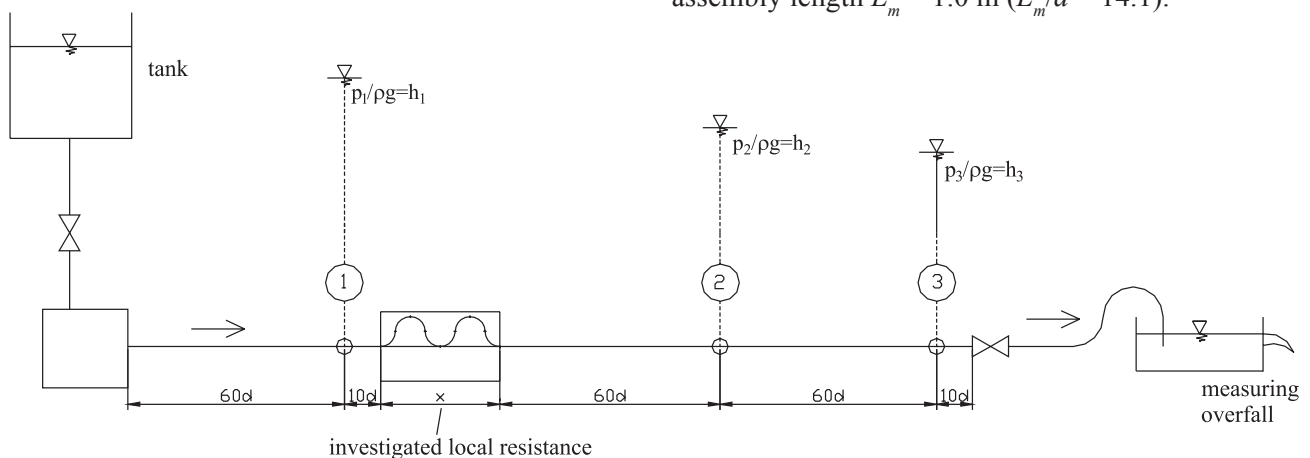

Fig. 1. Schematic diagram of measurements in the model

Needed results of the linear resistance coefficients of the studied pipelines yielded results which were found to be in quite good agreement with the ones calculated from the Prandtl-Karman formula (for hydraulically smooth pipes) and presented in (Cisowska 2004). The internal diameter of the polypropylene pipelines and pipe fittings was determined (by the volumetric method) to be $d = 71.0 \pm 0.1$ mm. Reynolds number range was $Re \in <47000, 248000>$.

3. Analysis and Interpretation of Local Resistance Experimental Results

Experimental local resistance coefficient values are usually given for the fully developed turbulent flow of liquid in the $25 \div 40\ d$ long section of the pipeline before the obstruction, taking into account the losses (due to the velocity and pressure distribution disturbances caused by the obstruction) along the $40 \div 70\ d$ long section after the obstruction. In practice, different local resistances are often closely spaced so that the flow of liquid cannot fully redevelop. Then the overall resistance coefficient for a system of pipe fittings is not equal to the direct sum of the individual resistance coefficients and it should be experimentally determined.

According to the Standard (Polish Standard 1976), $\zeta_{(2x90°)} = 2\zeta_{(90°)}$ for sequences of conformingly connected double elbows $\alpha_s = 2 \times 90° = 180°$, i.e. it is recommended to double the value of ζ_i of the individual elbows, whereas for alternatinvely connected double elbows the coefficient is $\zeta'_{(2x90°)} = 4\zeta_{(90°)}$. In neither case has this been corroborated by the results of the studies. The above recommendations result in overestimated local losses in the investigated pipe fittings (Tabl. 1 – series I, III and IV).

Generally, for the same ratio R/d, total numerical axial length l_o/d of elbows or bends, sum of central angles α_s and number of socket joints z, the hydraulic resistance of spiral-loop systems is much lower than that of sinusoidal-wave systems.

To generalize the experimental results for the systems of alternatively connected pipe fittings (including ones forming sinusoidal waves) an attempt of the a mathematical description of local resistance coefficient ζ as a function of the particular dimensionless similarity numbers was made. For this purpose the thirty two samples, possibilities of measurements relating to the systems of alternatively connected pipe fittings were divided into families depending on the segments' central angles $\alpha_i \in \{30°; 45°; 60°; 90°\}$.

By combining the families of relations ζ for $\alpha_i \in \{30°, 45°, 60°\}$ one obtains a sufficiently accurate

mathematical expression:

$$\zeta = -0.0756 + \frac{1.635}{(R/d)^3} - 0.00223\frac{\alpha_s}{\alpha_i} +$$
$$+0.780\frac{l_o}{d} - 0.823\,z \tag{1}$$

at a sum of the squares of the deviations of 0.055 and a standard deviation of 0.05. Relation (1) holds for the following intervals of dimensionless similarity numbers:

$$R/d \in <1.75,\ \ 4.25>;\ \ \alpha_s/\alpha_i \in <2.12>;$$
$$l_0/d \in <2.36,\ \ 35.60>;\ \ z \in <2,\ \ 32>.$$

For systems of alternatively connected pipe fittings at $\alpha_i = 90^0$ the following implicit formula for ζ:

$$\zeta = -0.0923 + \frac{2.437}{(R/d)^3} + 0.0654\frac{\alpha_s}{\alpha_i} +$$
$$+\frac{0.0648 \cdot (\alpha_s/\alpha_i)^2}{(R/d)^3} + 0.210\ \frac{l_o}{d} - 0.205\,z \tag{2}$$

at sum of the squares of the deviations of 0.072 and a standard deviation of 0.08 in parameter ranges: $R/d \in <1.0, 4.25>;\ \ \alpha_s/\alpha_i \in <2,\ \ 8>;$ $l_o/d \in <3.14;\ \ 53.41>;\ \ z \in <2,\ \ 48>$ is proposed.

Also the experimental results for ten geometric arrangements of conformingly connected elbows and bends ($\alpha_i = 90°$), including spiral loops, have been generalized. The following formula:

$$\zeta = 0.0891 + \frac{0.968}{(R/d)^3} + 0.0515\frac{\alpha_s}{\alpha_i} +$$
$$+0.170\frac{l_o}{d} - 0.168\,z \tag{3}$$
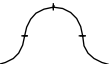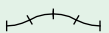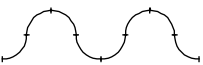
at sum of the squares of the deviations 0.056 and a standard deviation of 0.07 in parameter ranges: $R/d \in <1.0,\ \ 4.25>;\ \ \alpha_s/\alpha_i \in <2,\ \ 8>;$ $l_o/d \in <3.14,\ \ 28.27>;\ \ z \in <2,\ \ 24>$ is proposed.
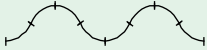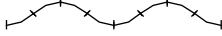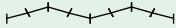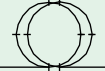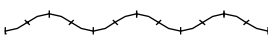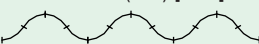
4. Conclusions

The local resistance coefficient of the studied systems consisting of (n) segmental elbows or bends considerably differs between conformingly connected systems and alternatively connected systems: in the former case the values of total resistance coefficient $\zeta_{(n)}$, which is not a direct sum of resistance coefficients ζ_i of the component pipe fittings, are much lower than in alternatively connected systems where the

Table 1. Measured local resistance coefficient for model ζ

Series	Description, scheme No. (α_i) $[\alpha_s]$	Variants A — systems of bends $\alpha = 15^0$ R/d = 4.25 ζ	Variants B — systems of bends $\alpha = 30^0$ R/d = 2.25 ζ	Variants C — systems of bends $\alpha = 45^0$ R/d = 1.75 ζ	Variants D — systems of elbows $\alpha = 90^0$ R/d = 1.00 ζ
I	Bends or elbows (90°) [90º]	0.279	0.324	0.434	–
II	Bends (45°) [45º]	0.178	–	–	–
III	2 conformingly connected bends or elbows (90°) [180º]	0.469	0.466	0.606	1.233
IV	2 alternatingly connected bends or elbows (90°) [180º]	0.426	0.561	0.856	2.841
V	2 alternatingly connected bends (60°) [120°]	0.313	0.401	–	–
VI	2 alternatingly connected bends (45°) [90°]	0.246	–	0.745	–
VII	2 alternatingly connected bends (30°) [60°]	0.150	0.276	–	–
VIII	4 bends or elbows (90°) [360°]	0.860	1.075	1.517	4.321
IX	4 bends (60°) [240°]	0.603	0.801	–	–
X	4 bends (45°) [180°]	0.462	–	1.174	–
XI	4 bends (30°) [120°]	0.282	0.459	–	–
XII	8 bends or elbows (90°) [720°]	1.974	1.977	2.996	7.994

XIII	8 bends 60° [480°]	1.438	1.444	–	–
XIV	8 bends 45° [360°]	0.976	–	2.109	–
XV	8 bends 30° [240°]	0.546	0.907	–	–
XVI	Spiral loop [360°] made from bends or elbows (90°)	0.830	0.700	1.120	1.781
XVII	2 spiral loops [720°] made from bends (90°)	–	1.352	1.655	–
XVIII a	12 bends (45°) [540°]	–	–	3.222	–
XVIII b	24 bends (30°) [720°]	–	2.330	–	–

hydraulic resistance of systems built from the same pipe fittings as above is much greater and $\zeta_{(n)}$ is approximately a direct sum of components ζ_i.

Ratio R/d and then equally central angle α_i (or ratio of central angles α_s/α_i), relative axial length l_o/d and number of socket joints z have the most significant effect on the local resistance coefficient of single segmental polypropylene elbows or bends and their systems.

The quantitative formulas for coefficient ζ derived in this paper can be used to polypropylene systems of bends and elbows or other plastics in the adopted range of dimensionless similarity numbers and systems of geometric similarity.

Notation

The following symbols are used in this paper:

d = the inside diameter of a pipeline or a pipe fitting;

l_o = the axial length of an elbow ($R/d \leq 1$) or a bend ($R/d > 1$): $l_{o(ni)} = (n_i\alpha°/360°)2\pi R$ or a system of such pipe fittings: $l_{o(n)} = (n\alpha_i°/360°)2\pi R$;

l_k = the length of the straight socket section in a segmental elbow or bend;

n = the number of a segmental elbows or bends (α_i) in a system (α_s);

n_i = the number of single elbow or bend (α) in segmental elbow or bend (α_i);

R = the radius of curvature of a segmental elbow or bend;

Re = the Reynolds number: $Re = \upsilon d/\nu$;

z = the number of socket joints in a segmental elbow or bend: $z = n_i$ or in a system: $z = n_i n$;

α = the central angle of a single elbow or bend;

α_i = the central angle of a segmental elbow or bend: $\alpha_i = n_i\alpha$;

α_s = the sum of central angles in a system of segmental elbows or bends: $\alpha_s = n\alpha_i$;

ζ = a nondimensional coefficient of local resistance.

References

[1] Cisowska I. (2004), *Studies of Hydraulic Resistance in Polypropylene Pipes and Pipe Fittings*, Wrocław University of Technology (doctoral) (in Polish).

[2] Kotowski A., Cisowska I. (2003), *Physical modeling of flows of liquid in hydraulically smooth pipes, 8th Conference on Hydraulic Engineering Problems,* Wrocław University of Technology, Wrocław-Kliczków, 4-6 June 2003 (in Polish).

[3] Polish Standard, PN-76/M-34034 (1976), Pipelines. Principles of calculating pressure losses (in Polish).

environment

Iwona Cisowska

Opory hydrauliczne w kształtkach z polipropylenu

1. Wstęp

Podane w literaturze wartości współczynników oporów miejscowych pojedynczych kolan ($R/d \le 1$) lub łuków ($R/d > 1$) odnoszą się głównie do kształtek stalowych i żeliwnych i znacznie odbiegają od wyników badań pojedynczych kształtek z tworzyw sztucznych, zwłaszcza w układach dwóch kolan lub łuków bezpośrednio po sobie występujących. Ze względu na to, że dotychczas nie przeprowadzono badań oporów miejscowych w takich układach, celem podjętych pomiarów było poznanie oporów miejscowych układów dwóch i więcej łuków lub kolan zgodnych (płaskich) połączonych szeregowo (w tym w postaci pętli) oraz oporów miejscowych układów dwu i więcej łuków bądź kolan przemiennych (w tym w postaci sinusoidalnych fal).

2. Metodyka badań

Badania modelowe oporów miejscowych dotyczyły 48 układów geometrycznych kolan oraz łuków segmentowych z PP, złożonych z kształtek o kątach środkowych $\alpha \in \{15°, 30°, 45°, 90°\}$ i względnych promieniach krzywizny $R/d \in \{1,0, 1,75, 2,25, 4,25\}$ oraz liczbie złączy kielichowych $z \in \langle 1,48 \rangle$, przy względnej długości prostek kielichowych $l_k/d = 0.70$. Średnicę wewnętrzną badanych rurociągów i kształtek z polipropylenu określono metodą objętościową w wysokości $d = 71,0 \pm 0,1$mm [1].
Schemat stanowiska doświadczalnego przedstawiono na rys. 1.

3. Analiza wyników

W układach zgodnych kolan podwójnych $\alpha_s = 2 \times 90° = 180°$ (występujących bezpośrednio po sobie) norma [2] podaje: $\zeta_{(2 \times 90^0)} = 2\zeta_{(90^0)}$, czyli zaleca podwajanie wartości ζ_i pojedynczych kolan, a w wypadku przemiennych kolan podwójnych – $\zeta'_{(2 \times 90^0)} = 4\zeta_{(90^0)}$. W badaniach nie potwierdzono takich zależności. Zalecenia te prowadzą do przeszacowania wartości strat miejscowych badanych

kształtek. Generalnie układy spiralnych pętli dają mniejszy opór hydrauliczny w porównaniu z układami w postaci sinusoidalnych fal dla danego stosunku R/d i tej samej sumarycznej długości osiowej l_o/d kolan bądź łuków, sumy kątów środkowych α_s oraz liczby złączy kielichowych z.

W uogólnieniu wyników badań układów przemiennych, w tym w postaci sinusoidalnych fal zbudowanych z kolan bądź łuków segmentowych, podjęto próbę opisu matematycznego współczynnika oporu miejscowego ζ w funkcji czterech bezwymiarowych liczb podobieństwa.

Z połączenia rodzin zależności ζ dla układów przemiennych złożonych wyłącznie z łuków segmentowych, przy $\alpha_i \in \{30°; 45°; 60°\}$, uzyskano zadowalająco dokładny zapis matematyczny w postaci:

$$\zeta = -0.0756 + \frac{1.635}{(R/d)^3} - 0.00223 \frac{\alpha_s}{\alpha_i} + \\ +0.780 \frac{l_o}{d} - 0.823\, z \tag{1}$$

przy sumie kwadratów odchyleń równej 0,055 i odchyleniu standardowym równym 0,05. Zależność (1) obowiązuje dla przedziałów bezwymiarowych liczb podobieństwa, związanych z zakresem przeprowadzonych badań, a mianowicie:

$$R/d \in \langle 1,75; \quad 4,25 \rangle; \quad \alpha_s/\alpha_i \in \langle 2.12 \rangle;$$
$$l_0/d \in \langle 2,36; \quad 35,6 \rangle; \quad z \in \langle 2, \quad 32 \rangle.$$

Dla układów przemiennych, przy $\alpha_i = 90°$, proponuje się następującą, uwikłaną postać wzoru do obliczeń ζ:

$$\zeta = -0.0923 + \frac{2.437}{(R/d)^3} + 0.0654 \frac{\alpha_s}{\alpha_i} + \\ + \frac{0.0648 \cdot (\alpha_s/\alpha_i)^2}{(R/d)^3} + 0.210 \frac{l_o}{d} - 0.205\, z \tag{2}$$

przy sumie kwadratów odchyleń równej 0,072 i odchyleniu standardowym równym 0,08; w zakresie zmian parametrów:

$$R/d \in \langle 1,0; 4,25 \rangle; \quad \alpha_s/\alpha_i \in \langle 2, \quad 8 \rangle;$$
$$l_0/d \in \langle 3,14; \quad 53,4 \rangle; \quad z \in \langle 2, \quad 48 \rangle.$$

Uogólniono także wyniki badań współczynnika ζ dla układów geometrycznych kolan i łuków segmentowych zgodnych ($\alpha_i = 90^0$), w tym tworzących spiralne pętle. Zaproponowano następującą postać wzoru:

$$\zeta = 0.0891 + \frac{0.968}{(R/d)^3} + 0.0515 \cdot \alpha_s / \alpha_i +$$
$$+0.170 \cdot l_o / d - 0.168 \cdot z \tag{3}$$

przy sumie kwadratów odchyleń 0,056 i odchyleniu standardowym równym 0,07, w zakresie zmian wartości liczb podobieństwa:

$$R/d \in <1,0; \quad 4,25>; \quad \alpha_s / \alpha_i \in <2; \quad 8>;$$
$$l_o/d \in <3,14; \quad 28,27>; \quad z \in <2; \quad 24>$$

4. Podsumowanie

Współczynnik oporów miejscowych badanych układów (n) kolan bądź łuków różni się zasadniczo dla układów płaskich i przemiennych. W układach płaskich występują mniejsze wartości sumarycznego współczynnika oporu układu $\zeta_{(n)}$, który nie jest sumą prostą wartości współczynników oporów ζ_i – składowych kształtek, w przeciwieństwie do układów przemiennych, gdzie występuje większy opór hydrauliczny układów, a $\zeta_{(n)}$ jest w przybliżeniu sumą prostą składowych ζ_i.

Najistotniejszy wpływ na wartość współczynnika oporów miejscowych pojedynczych kolan lub łuków z PP oraz ich układów, ma stosunek względnej krzywizny kształtki R/d, a następnie równorzędnie: kąt środkowy α_i (lub stosunek α_s/α_i), względna długość osiowa l_o/d i liczba złącz kielichowych z. Wyprowadzone w pracy wzory ilościowe na wartość współczynnika ζ odnoszą się do badanych układów kształtek z PP, a także innych tworzyw sztucznych pod warunkiem zachowania podobieństwa geometrycznego i wartości bezwymiarowych liczb podobieństwa wynikających z zakresu przeprowadzonych badań oraz przyjętych założeń.